Title: Immunofocusing on the conserved fusion peptide of HIV envelope glycoprotein in rhesus macaques

Payal P. Pratap[1,2], Christopher A. Cottrell[2,3], James Quinn[2,4], Diane G. Carnathan[5], Daniel L.V. Bader[1,2,3], Andy S. Tran[1], Chiamaka A. Enemuo[5], Julia T. Ngo[5], Sara T. Richey[1], Hongmei Gao[6], Xiaoying Shen[6], Kelli M. Greene[6], Jonathan Hurtado[2,3], Katarzyna Kaczmarek Michaels[7], Elana Ben-Akiva[7], Ashley Lemnios[3], Mariane B. Melo[2,3,8], Joel D. Allen[9], Gabriel Ozorowski[1,2], Max Crispin[9], Bryan Briney[2,3], David Montefiori[6], Guido Silvestri[5], Darrell J. Irvine[2,7,8,10], Shane Crotty[2,3], and Andrew B. Ward[1,2*]

Author Affiliations

[1] Department of Integrative Structural and Computational Biology, The Scripps Research Institute, La Jolla, CA 92037, USA

[2]Center for HIV/AIDS Vaccine Development (CHAVD), The Scripps Research Institute, La Jolla, CA, 92037, USA

[3] Department of Immunology and Microbiology, The Scripps Research Institute, La Jolla, CA 92037, USA

[4]La Jolla Institute for Immunology, La Jolla, CA 92037, USA

[5]Division of Microbiology and Immunology, Emory National Primate Research Center, Emory University, Atlanta, GA 30329, USA.

[6]Duke Human Vaccine Institute and Department of Surgery, Duke University Medical Center, Durham, NC, USA.

[7]Koch Institute for Integrative Cancer Research, Massachusetts Institute of Technology, Cambridge, Massachusetts 02139, USA

[8]Howard Hughes Medical Institute, 4000 Jones Bridge Rd., Chevy Chase, MD, 20815

[9]School of Biological Sciences, University of Southampton, Southampton, SO17 1BJ, UK

[10]Department of Biological Engineering, Massachusetts Institute of Technology, Cambridge, Massachusetts 02139, USA

[*]Correspondence: andrew@scripps.edu

Abstract/Summary

During infection, the fusion peptide (FP) of HIV envelope glycoprotein (Env) serves a central role in viral fusion with the host cell. As such, the FP is highly conserved and therefore an attractive epitope for vaccine design. Here, we describe a vaccination study in non-human primates (NHPs) where glycan deletions were made on soluble HIV Env to increase FP epitope exposure. When delivered via implantable osmotic pumps, this immunogen primed immune responses against the FP, which were then boosted with heterologous trimers resulting in a focused immune response targeting the conserved FP epitope. Although autologous immunizations did not elicit high affinity FP-targeting antibodies, the conserved FP epitope on a heterologous trimer further matured the lower affinity, FP-targeting B cells. This study suggests using epitope conservation strategies on distinct Env trimer immunogens can focus humoral responses on desired neutralizing epitopes and suppress immune-distracting antibody responses against non-neutralizing epitopes.

47 **Introduction**

48 Broadly neutralizing antibodies (bnAbs) against HIV-1 envelope glycoprotein (Env) have
49 been isolated from patients infected with HIV, but only after prolonged periods of infection and
50 with extensive somatic hypermutation[1–3]. As the only protein expressed on the viral surface, Env,
51 a heterotrimer of gp120 and gp41 subunits, has been the target of many vaccine efforts[4–8]. An
52 efficacious vaccine regimen needs to prime and affinity mature bnAb responses against multiple
53 conserved neutralizing epitopes on Env. The fusion peptide (FP) is critical for viral membrane
54 fusion[9] and consists of a conserved 15-20 amino acid long hydrophobic motif starting at the N-
55 terminus of gp41 subunit of Env[10–15]. The FP neutralizing epitope is sterically occluded by 4
56 canonical glycans at positions N88, N230, N241 and N611[13]. FP is a viable target for HIV vaccine
57 design efforts as potent bnAbs VRC34.01, PGT151, and ACS202 against the FP have been isolated
58 from human elite neutralizers[11,16–18].

59 Multiple vaccination efforts in non-human primates (NHP), rabbits and mice have elicited
60 antibodies (Abs) that bind to the FP with a range of neutralizing and protective capabilities[10,13,15,19–
61 23]. Consistent elicitation of FP-targeting Abs has been achieved by removal of specific canonical
62 FP N-linked glycans in priming immunogens[13,23]. One such study immunized NHPs with
63 BG505.SOSIP with three out of four canonical FP glycans removed except the glycan at residue
64 N88[23], a critical N-glycan for binding of FP-targeting bnAb VRC34.01[11]. The study showed that
65 NHPs immunized with autologous trimers of increasingly native FP N-glycan presentation
66 developed Abs that recognize the FP. Structural analysis of elicited polyclonal Ab responses,
67 however, indicated that deletion of several glycans around the FP biased Ab recognition and
68 maturation towards the glycan deletion at N611, thereby greatly limiting the potential for
69 neutralization breadth and potency.

70 To overcome these limitations, we employed several immunofocusing strategies to our
71 prime and boost immunogens to present the FP epitope in a more native-like context. We first
72 immunized NHPs with recombinant BG505- and CH505-based chimeric immunogens either with
73 full FP glycan occupancy (+N241) or with a single FP N-glycan deletion (ΔN241), to increase
74 epitope accessibility in a more conservative manner than our prior approach[23]. Primed responses
75 were first boosted with the BG505-CH505+N241 chimeric antigen and later boosted with a
76 different trimer genotype with an identical FP to focus immune responses on the FP. Slow delivery
77 immunization via osmotic pumps was employed for the priming phase to enhance generation of
78 neutralizing antibodies (nAbs) as well as germinal center (GC) activity[20,24]. FP-specific GC B cell
79 populations were observed over the course of the study as well as overall antigen specificity and
80 memory B cell (MBC) population dynamics. Negative stain electron microscope polyclonal
81 epitope mapping (nsEMPEM) was performed on animal plasma two or four weeks post
82 immunization to map polyclonal Abs (pAbs) responses[25]. CryoEMPEM was later used to
83 characterize pAbs at higher resolution to delineate residue level interactions with the immunogen
84 to better comprehend the immunogenicity of the antigens used in the study[23,26]. Overall, while we
85 did not observe robust FP priming and neutralization activity from this study, the techniques and
86 tools used for polyclonal response evaluation have important implications for epitope-based
87 vaccine research.
88

89 **Results**

90 **FP Targeting Immunogen Design and Immunization regimen**

91 Previous FP studies with non-glycosylated trimers around the FP have resulted in Ab
92 responses biased towards the glycan deletions[13,23]. Instead, we hypothesized that a more

93 conservative glycan deletion approach would induce FP-specific responses capable of broad HIV-
94 1 coverage. In this study, we primed NHPs using chimeric trimers based on BG505 and CH505
95 with the V1, V2, V3, and V5 loops of CH505[27], a clade C virus, grafted onto a clade A BG505
96 trimer background as wild-type BG505 does not carry two of the four canonical FP glycans at
97 positions N241 and N230[28,29]. BG505 also lacks a conserved glycan at position 289, which opens
98 up an epitope previously shown to be immunogenic, so we introduced a glycan at position 289 to
99 mitigate the immunodominance of this glycan hole epitope (Fig 1a)[29]. In the experimental group,
100 the chimeric priming immunogen presented three of the four FP glycans: N611, N88 and N230
101 but lacking in the N241 glycan (BG505-CH505ΔN241) (Fig 1a). Alternatively, the control group
102 was primed with an autologous, chimeric immunogen with all four canonical FP glycans present,
103 including N241 (BG505-CH505+N241). For the priming period, both groups of animals were
104 given their respective soluble antigens and adjuvants via continuous delivery via an osmotic pump
105 over a four-week period at a dose of 100 ug of antigen and 750 ug of SMNP adjuvant (Fig
106 1b)[23,24,30]. All subsequent immunizations were given as bolus with the same dosages. The animals
107 were first boosted with the BG505-CH505+N241 immunogen at week 12 and later boosted with a
108 heterologous, clade B trimer, AMC016[31], but with BG505 FP sequence grafted, to further
109 immunofocus on the FP and suppress boosting of pre-existing Abs against off-target epitopes (Fig
110 1b). The AMC016 trimer is highly glycosylated and therefore suitable to suppress BG505-CH505-
111 specific off-target and glycan hole-directed pAb responses[29,32,33]. AMC016 has previously been
112 shown to induce strain-specific, neutralizing Abs in rabbits after autologous immunizations[31].

113 To shield an otherwise immunodominant epitope at the base of soluble Env trimers, non-
114 native N-glycans were introduced at positions 656 and 660 (Fig 1c) in all the constructs. Previous
115 research has shown that membrane-bound trimers have higher glycan occupancy and improved

116 glycan processing than soluble trimers due to longer retention in the ER/Golgi[34,35]. Here we
117 employed an analogous strategy to extend the C-terminus of Env by introducing a Furin cleavage
118 site (RRRRRR)[36] after residue 664 of gp41, followed by a GS-rich linkage to a 3x-Flag-Tag
119 (priming immunogens) or a 9x-Flag-Tag (boosting immunogens). This tag increases the
120 translation time and is subsequently cleaved off by Furin protease and is therefore not present in
121 the final immunogen (Fig S1a).

122 When a 3x-Flag-Tag was used, the introduced glycan at the C-terminus of gp41, N656 was
123 less than 40% occupied while N660 remained completely unoccupied (Fig 1c). When a 9x-Flag-
124 Tag was used, the glycan at N656 was ~75% occupied, while glycan occupancy at N660 remained
125 0%. In these constructs there was also a large change in the glycan occupancy at canonical gp41
126 glycan at 625, which historically has low occupancy when expressed as a soluble trimer truncated
127 at position 664 with a stop codon[37]. In the 3x-Flag-Tag constructs, the glycan at position 625 was
128 completely unoccupied. However, in the autologous and heterologous boosting immunogens,
129 which have 9x-Flag-Tags, there was a significant increase in glycan occupancy at position 625 to
130 40% in the BG505-CH505+N241 autologous boost and 98% in the AMC016 heterologous boost
131 (Fig 1c). Although a PNGS sequon at N230 was present in the Env sequence for the BG505-
132 CH505ΔN241 construct, mass spec analysis of this glycan site was unable to determine the
133 occupancy levels of this FP glycan and so the occupancy of this site remains unknown.

134 Historically, BG505 SOSIP.664 has introduced cysteine residues at positions 501 of gp120
135 and 605 of gp41, forming an intra-protomer disulfide bond that stabilizes recombinant native-like
136 Env trimers[28]. Despite this Env stabilization effort, antibody-mediated immunogen disassembly
137 has been observed after repetitive autologous trimer immunizations[38]. Therefore, we introduced a
138 new disulfide linkage in the BG505-CH505ΔN241 and BG505-CH505+N241 constructs, 501C-

139 L663C, to prevent in-vivo trimer disassembly. Notably, this disulfide prevents binding of
140 RM20A3, a base binding mAb isolated from macaques that were repeatedly immunized with
141 BG505-based constructs (Figs S1b and S1c)[12,38,39]. The AMC016 construct has the cysteines at
142 positions 501 of gp120 and 664 of gp41, which also prevent RM20A3 binding (Figs S1b and S1c).

143 **NsEMPEM detected FP response after heterologous boosting**

144 Prior studies using EMPEM to map pAbs against different epitopes of the HIV Env protein
145 provide a basis to evaluate the success of our immunofocusing approach [12,26,40]. Here, we used
146 nsEMPEM to analyze pAb responses at post immunization timepoints using probe antigens
147 matched to the most recent immunogen (Fig 2a and Fig S2a)[25]. At week 4 only base binders were
148 bound to the probing antigens, in this case the priming immunogens, in each group (Fig 2a and Fig
149 S2a). This result aligns with previous observations showing base responses are consistently elicited
150 early in soluble Env trimer immunizations in animal and human studies[12,23–26,40,41].

151 After the initial priming immunizations, both groups were boosted with an autologous,
152 chimeric immunogen with all four FP glycans present, BG505-CH505+N241, the same
153 immunogen given to the control group for priming (Fig 1). Week 14 nsEMPEM analysis revealed
154 more epitopes detected relative to week 4 (Fig 2a and Fig S2a). In addition to base binding pAbs,
155 we observed pAbs bound to the C3/V5 region and V1/V2 region in most animals in both groups.
156 One animal in the experimental group, LJ66, also developed a gp120/gp120 interface (IF) response
157 (Fig S2a). One animal in the control group, RUu18, revealed an FP response (Fig S2a), however,
158 follow-up cryoEM (discussed below) and FP-ELISA (Fig 2b, green triangle) demonstrated that the
159 FP response observed in RUu18 via nsEMPEM did not specifically target the FP.

160 While FP pAbs were detected as early as six weeks in our earlier 2018 NHP study[23], FP
161 targeting pAbs were not observed via nsEMEPM until 4 weeks after the heterologous AMC016
162 trimer boosts at weeks 24 and 39 in the majority of animals within the experimental and control
163 groups, respectively, in this study (Fig 2a and Fig S2a),. This suggests removal of only the N241
164 glycan around the epitope does not induce a robust priming immune response against the FP.
165 Although FP responses were not observed at the earlier time points, FP-ELISA data suggested FP-
166 recognizing Abs were elicited at low levels during chimeric BG505-CH505 construct
167 immunizations (Fig 2c and Fig S2b).

168 Week 28 nsEMPEM analysis of the experimental group animals revealed base and FP
169 responses, and one animal, LJ66, additionally showed a gp120/gp120 IF response (Fig 2a and Fig
170 S2a). The control group, which had received three immunizations of the BG505-CH505+N241
171 antigen by this point, still exhibited base, V1/V2/V3, and V5 responses in all the animals. Two
172 animals in the control groups revealed gp120/gp120 IF responses and FP responses, respectively,
173 via nsEMPEM analysis. While our data suggests that a single canonical FP glycan deficiency on
174 Env does not prime a robust FP response compared to a fully glycosylated trimer, the results from
175 the heterologous AMC016 boost were encouraging.

176 To distinguish if post-AMC016 boost FP elicitation in the experimental group was due to
177 epitope accessibility in the priming immunogens or introduction of the heterologous boosting
178 immunogen, both groups were immunized a fourth and final time with the heterologous AMC016
179 trimer at week 39. NsEMEPM analysis of week 43 plasma samples in the control groups showed
180 elicitation of FP-targeting Abs in five of the six control animals (Fig 2a). The experimental group,
181 which had received two immunizations of the AMC016 trimer, elicited FP and base responses, as

182 observed in week 28, however most of the animals now also exhibited AMC016-specific C3/V5
183 responses. Strain-specific responses after autologous immunizations but not after heterologous
184 immunizations is a commonly observed phenomenon in multiple viral vaccination platforms[42,43].
185 Although nsEMPEM suggested both groups showed FP-directed responses after heterologous
186 boosting, FP-ELISA showed that the experimental group had significantly higher recognition of
187 the FP, suggesting that the N241 glycan hole in the BG505-CH505ΔN241 immunogen did impact
188 FP-specific responses later boosted by the heterologous AMC016 trimer (Fig 2c and Fig S2b).
189 Serum ELISAs showed negligible differences between experimental and control group
190 antibody titers against the BG505-CH505+N241 probing antigen throughout the duration of the
191 study (Fig 2d). However, the experimental group antibody titers had better AMC016 recognition
192 after heterologous boosting at week 24, compared to the control group, even after the control group
193 was heterologously boosted at week 39 (Fig 2e).
194 **Cross-reactive immunity observed via nsEMPEM**
195 Cross-linking nsEMPEM of polyclonal sera enables detection of lower abundance
196 antibodies[44]. Hence, prior to heterologous boosting we attempted this approach to reveal which
197 epitopes might be boosted at weeks 24 and 39. The 2D class averages of samples cross-linked with
198 the heterologous trimer suggests FP-recognizing Abs are present in plasma, which had not been
199 observed in nsEMPEM analysis with BG505-CH505+N241 trimer (non-crosslinked) (Table S1).
200 This suggestion was corroborated by the FP-ELISA data that showed FP-recognizing pAbs at the
201 week 14 and 28 time points in both groups (Fig 2c). Thus, FP-directed Abs were elicited at low
202 abundance and/or low affinity levels in the serum by the autologous immunogens. In all the
203 animals, the 2D class averages also show the presence of a base-binding Ab that was able to cross-
204 link with the heterologous immunogen prior to its immune exposure (Table S1). These

205 observations suggest that cross-linked nsEMPEM analysis can reveal cross-linking epitopes
206 between heterologous antigens and can be a valuable tool for vaccine design and boost immunogen
207 selection for real time study evaluation[45].
208

209 **Flow Cytometry Analysis Did Not Reveal Remarkable Changes in GC Populations**

210 To gain visibility of the GC dynamics over the course of immunization, longitudinal lymph node
211 fine needle aspirates (FNAs) were performed on the draining inguinal lymph nodes of each animal
212 at several timepoints throughout the study (Fig S3). Cells collected during the FNAs were stained
213 and analyzed using flow cytometry (Fig 3). Overall, GC B cell and TFH cell responses were
214 observed in the sampled lymph nodes after initial priming and after the final boost (Fig 3a and 3b).
215 GC response (as measured by GC B cell and TFH cell percentage) was largely unchanged after
216 the boosts at weeks 12 and 24. Beginning at week 24, in addition to surface marker staining, FNA
217 cells were also stained with a fluorescent probe of the heterologous boost immunogen.
218 Interestingly, in the experimental group, the percentage of GC B cells collected from the lymph
219 nodes that are positive for the heterologous AMC016 trimer are greater at week 24 than week 28,
220 four weeks post-heterologous boost (Fig 3c). Despite no immunization with the AMC016 trimer,
221 the control group exhibited a slight increase in heterologous AMC016 trimer recognition after
222 BG505-CH505+N241 trimer boosts at week 24 (Fig 3c).
223

224 **Serum Neutralization Detected After AMC016 Heterologous Boosting**

225 We assessed heterologous or autologous neutralization of serum samples longitudinally
226 using three pseudovirus (PV) neutralization panels: a PV panel sensitive to FP-targeting bnAbs, a
227 BG505- and a CH505-specific mutant PV panel (Fig 4a, 4b, and 4c, respectively) (Tables S2, S3,

228 and S4, respectively). The former is comprised of ten heterologous PVs selected for their
229 neutralization sensitivity to FP-specific bnAbs[10,23]. Week 14 serum neutralization analysis
230 revealed sporadic and weak neutralization for the FP sensitive panel, though slightly stronger
231 against 3988.25 Tier 2 PV (Fig 4a; top panel). There was no detectable neutralization against
232 BG505 and relevant mutant panel, except for two animals, one from each of the groups, that
233 showed weak neutralization against the N611A mutant PV, which does not have a glycan present
234 at position 611 of gp41 (Fig 4b; top panel). When tested against the CH505 PV panel, there was
235 detectable neutralization against the Tier 2 transmitter/founder (TF) virus and against the Tier 1A
236 w4.3 virus for the animals in both groups except 1 RM in the control group (Fig 4c).

237 Week 28 serum samples were analyzed for neutralization. One animal, RQk18, from the
238 experimental group neutralized six of the nine PVs of the FP sensitive panel, all of which contained
239 FP sequence identical to the FP sequence used in the immunogens of this study (Fig 4a; middle
240 panel and Table S2). None of the control animals nor the rest of the experimental group developed
241 cross-neutralizing capabilities for the viruses assessed in the FP panel except weak neutralization
242 of Tier 2 3988.25 virus (Fig 4a; middle panel). Among the control group animals, none of them
243 neutralized the BG505 PVs except weakly against the Tier 2 N611A PV seen in two of the animals
244 (Fig 4b; middle panel). Within the experimental group, one animal, RQk18, neutralized five of six
245 BG505 PV panel and four out of the six animals neutralized the N611A PV (Fig 4b; middle panel
246 and Table S3). There was less serum neutralization of CH505 TF PV among the experimental
247 group at this time point compared to the control group, which is expected since the experimental
248 group received AMC016 trimers, and control received the BG505-CH505+N241 chimeric
249 immunogen at week 24 (Fig 4c and Table S4).

250 After the week 39 boost with AMC016 trimer, FP responses were observed via nsEMPEM
251 in both experimental and control groups in five out of six animals (Fig 2a). At week 43, one animal
252 in the control group weakly neutralized one of nine PVs on the FP sensitive panel (Fig 4a; bottom
253 panel and Table S2) and five of the six mutant BG505 panel (Fig 4b; bottom panel and Table S3).
254 After this second AMC016 immunization, two more animals in the experimental group were able
255 to neutralize additional PVs in the BG505 panel (Table S3) but animal RQk18 continued to weakly
256 dominate in the FP sensitive panel neutralization with two other animals showing even weaker
257 neutralization capacity (Table S2).
258 To test whether the weak serum neutralization profiles observed were mediated through
259 FP recognition, we conducted an FP competition neutralization assay on a subset of PVs, whereby
260 serum samples were titrated with FP-peptide, to capture any FP-recognizing antibodies in the
261 serum (Fig S4 and Table S5). FP-peptide titration with VRC34.01 positive control showed
262 significant decrease in PV neutralization, however, there was no impact on the serum
263 neutralization profiles from immunized animals. The FP competition neutralization results suggest
264 that the weak serum neutralization observed in a subset of the animals in the larger subset of PVs
265 tested were due to non-FP directed neutralization.
266
267 **CryoEMPEM analysis reveals high resolution on-target and off-target immune responses**
268 To better understand the types of FP region responses that were elicited in the animals and
269 overall immunogenicity of our constructs, we conducted cryoEMPEM analysis[23,26] on two animals
270 - RQk18 at week 43 and RUu18 at week 14 time points (Fig S5 and Table S6) - to define the
271 molecular interactions between antigen and pAb. Animal RQk18 developed weak neutralization
272 breadth among the heterologous FP-sensitive PV panel after week 24 boosts, which persisted

273 through the week 39 boosts. CryoEMPEM analysis of RQk18 week 43 fab response complexed
274 with the heterologous AMC016 trimer resulted in three high-resolution maps: 2 define distinct
275 pAb classes targeting the base of the trimer and one shows a pAb bound to the FP (Fig S5a).
276 Animal RUu18 exhibited what appeared to be an "FP" response via nsEMPEM at week 14 despite
277 FP-ELISA indicating poor FP recognition among the polyclonal IgG responses (Fig 2c, green
278 triangle and Fig S2a). Multiple classes of pAbs were classified that targeted off-target BG505-
279 CH505 epitopes: the base, V1V2V3 region and the non-specific "FP" (Fig S5b).

280 ***RQk18 week 43 - FP***

281 Animal RQk18 elicited a heterologous, neutralizing Ab response after week 24 AMC016
282 trimer boost, as determined by neutralization assays (Fig 4). To determine whether we could
283 interpret high-resolution structural data and infer sequence information of the bound, polyclonal
284 Abs, we turned to cryoEMPEM, which revealed two epitopes targeted after boosting with the
285 heterologous trimer - the FP and base (Fig S5a). We resolved a 3.1 Å map with well-resolved
286 density for the FP epitope as well as the variable region of the pAb, RQk-FP-A (Fig 5a).

287 The structural analysis revealed a fully resolved N-terminus of the FP, stabilized by
288 aromatic side chains on the heavy and light chains of the Ab (Fig 5b). The HCDR3 of the heavy
289 chain had a high abundance of aromatic residues, which help to stabilize the FP, a highly
290 hydrophobic region (Fig 5b). This hydrophobic string of aromatic residues in the HCDR3 feature
291 has been observed in two other bnAbs that target the FP - PGT151 and ACS202[18,46]. Such evidence
292 indicates that NHPs are capable of eliciting FP Abs that have similar features to FP-directed human
293 bnAbs. Apart from the HCDR3, the heavy chain contacts to the trimer include the CDR1 and
294 CDR2 loops and a few residues of the framework region (FWR) 3 region. The light chain helps

295 stabilize the N-terminus of the FP via CDRL3 loop interactions. Contacts with canonical FP Ab
296 contacts as mentioned earlier were also observed for this pAb (Fig 5c).

297 ***RUu18 week 14 - C1/C2 non-specific "FP" adjacent responses***

298 Prior structural analysis of neutralizing, FP-targeting Abs have shown that the N-terminus
299 of the FP is not typically resolved unless stabilized by an Ab[10,11,13,23]. NsEMPEM suggested animal
300 RUu18 mounted an FP response by week 14 of the study, but an FP-specific ELISA suggested
301 little FP interaction (Fig S2a and Fig 2c, green triangle). This indicated that there were
302 immunogenic residues near the FP epitope that could not be resolved from true FP responses at
303 low resolution. At high resolution, the "FP" Ab did not show engagement with the N-terminus of
304 the FP (Fig 5d). Rather, the first FP residue observed interacting with RUu-FP-1 pAb is L520 (Fig
305 5e). The pAb instead predominantly interacted with the following residues: E83 main chain
306 (99.5% global prevalence), I84 (45.21% prevalence), V85 (39.04% global prevalence), E87
307 (56.06% global prevalence), K231 (81.26% global prevalence), M535 (13.72% global prevalence).
308 Previous epitope analysis of anti-FP bnAbs has shown that these non-FP residues commonly
309 interact with anti-FP Abs[23], consistent with the high overlap with the FP epitope despite lack of
310 specific recognition of the FP N-terminus. Although this response was not visualized for the other
311 control group members at week 14, FP-ELISA titers and nsEMPEM of week 43 results for the
312 control group suggests cross-reactivity of C1/C2-partial FP response within all the control groups
313 members and one of the experimental groups (LJ66) (Figs 2c and S2).

314 ***RUu18 week 14 - V1V2V3***

315 Three different V1V2V3-targeted pAbs maps were resolved to ~4 Å from cryoEMPEM
316 analysis of RUu18 at week 14 (Fig S6). Although this Ab response was not observed at the week
317 4 nsEMPEM analysis in either group, complexing polyclonal fabs isolated from week 14 with the

318 BG505-CH505ΔN241 antigen showed binding of a V1V2V3 Ab to the priming trimer. Glycan
319 analysis of the immunogens revealed an under occupancy of conserved glycans near the variable
320 loops of gp120 of the boosting immunogen used at the week 12 boost for both groups (Fig 1c).
321 Two of the three maps revealed a hydrophobic pocket that was created by hydrophobic residues in
322 the substituted V1, V2, and V3 loops (Fig S6b). The HCDR3 of the Ab wedges between the loops
323 to interact with a hydrophobic pocket formed by residues: A134, A136, I142, L175, V323 and
324 I326. However, these maps also revealed the lack of glycosylation at a highly conserved, PNGS at
325 residue N156 of the trimer-associated mannose patch (TAMP) (Fig S6c)[47]. Another 3.9 Å map,
326 RUu-V1V2V3-5, showcases the HCDR3 of another Ab interaction with the variable loop
327 hydrophobic region mentioned above, but in this case the presence of the N156 glycan would clash
328 with the HCRD1 of this Ab instead of the light chain as in RUu-V1V2V3-2 (Fig S6d and S6c,
329 respectively). Although the glycan sub-occupancy observed was unforeseen, the glycan hole and
330 hydrophobic residues, synergistically, make this V1V2V3 region immunogenic and potentially
331 distract from on-target responses.

332 ***RUu18 week 14 - Base***

333 A 4.1 Å map of a base Ab, RUu-Base-4 revealed an epitope that targeted the tryptophan
334 clasp via HCDR1 and HDCR2 loops with long HCDR3 interactions with the N-terminus of gp120
335 (Fig S7a (left panel) and S7b). This epitope response was surprising as both autologous and
336 heterologous immunogens in this study were shown to not bind RM20A3 (Figs S7a (middle panel)
337 and S7c) via BLI analysis (Fig S1b). The lack of detectable RM20A3 binding initially led us to
338 believe in the lack of exposure for this epitope in this construct, suggesting potential inaccessibility
339 of this tryptophan clasp to immune recognition in-vivo. However, the adaptive immune system,

340 unsurprisingly, adapted and targeted this neo-epitope and was able to accommodate the disulfide
341 bond at the base of the trimer.

342 ***RQk18 week 43 - Base***

343 Two maps of AMC016 SOSIP bound by base Abs were also resolved during the analysis
344 of RQk18 week 43 cryoEMPEM. A map with a base Ab, RQk-Base-C, was resolved to 3.1 A and
345 also revealed an epitope that resembled the epitope of RM20A3 (Figs S7a, S7c and S7d)[12,48]. The
346 epitope similarity between the two polyclonal complexes at this region suggests a conservation of
347 the Ab response against this hydrophobic pocket at the base of the trimer (Fig S7a). A particularly
348 well-resolved 2.9 Å map, RQk-Base-A, revealed an Ab that interacted heavily with the charged
349 glutamic acid residues at the N-terminus of gp120 in AMC016 soluble trimer at positions E32,
350 E32a, and E33 (Fig S7e). While we had hypothesized that the base of the trimer may be less
351 targeted by antibodies with the introduction of the inter-protomer disulfide linkages, EMPEM
352 results showed that the base of the trimer remained relatively immunodominant, although less
353 susceptible to antibody induced disassembly due to the introduced disulfides.

354

355 **Structure To Sequence of RQk-FP**

356 The quality of the 3.1 Å map of RQk-FP-A allowed for structure to sequence (STS) analysis
357 to infer the amino acid sequence of the Ab based on the map characteristics and isolate FP-specific
358 mAbs[49]. We were able to assign highest confidence scores for paratope residues and infer putative
359 heavy- and light-chain sequences (Supp Data 01 and 02). PBMCs from week 42 for animal RQk18
360 were sequenced. The sequencing data and high resolution of the epitope-paratope interface enabled
361 the design of four heavy chain and two light chain sequences that appeared to converge best with
362 the highest confidence assignment regions. Sequencing analysis revealed the heavy chain to be of

363 IGHV4-117*01 and IGHD2-12*01 allelic usage. Sequence analysis from week 14 PBMCs for
364 animal RQk18 indicated that while IGHV4-117*01 and IGHD2-12*01 genes were used in
365 different immunoglobulin (Ig) detected at this pre-heterologous boost time point, these genes were
366 not paired in any of the 2170 clonotypes sequenced at this time point (Supp Data 03).

367 We designed a panel of eight monoclonal antibodies (mAbs) by pairing the four distinct
368 heavy-chains with both light-chains and assessed binding kinetics against autologous and
369 heterologous trimers, and subsequent nsEMPEM analysis (Tables S7-S9). Four out of eight mAbs
370 showed detectable binding to the BG505-CH505+N241 and AMC016 Boost constructs, the
371 majority of which showed higher affinity for BG505-CH505+N241 Boost (Fig 6a and S8a).
372 Interestingly, FP-ELISA of the RQk-FP mAbs showed that the highest FP bindings mAbs showed
373 reduced trimer recognition in the BLI results, suggesting these antibodies bound the FP
374 productively the 3D spatial restraints within the trimer reduced FP binding (Fig 6b). Negative stain
375 analysis of these trimer binding mAbs indicated that they did bind to the FP region of the trimer
376 (Fig S8b). We undertook cryoEM with mAb 05, which had the best profile for affinity for the
377 trimers (Fig 6a and S8a). A 3.9 Å map of RQk-FP-mAb-05 in complex with AMC016 and PGT122
378 (Fig 6c) showcases a similar binding mode to the pAb map (Fig 5A). When the model of pAb
379 RQk-FP-A was docked in into the map of RQk-FP-mAb-05, there was a high degree of overlap of
380 the FP antibody model and the FP mAb 05 density (Fig 6d). However, the N-terminus of the FP
381 confirmation from pAb RQk-FP-A did not fit well into the FP density of RQk-FP-mAb-05 with
382 the N-terminus not as clearly resolved (Fig 6e). The mAbs that showed binding to the immunogens
383 via BLI were subjected to neutralization assays to determine whether the designed mAbs could
384 recapitulate serum neutralization capacity. The mAbs were determined to be non-neutralizing (Fig
385 6f, Tables S10-S11), suggesting that the FP was not the neutralizing epitope seen in serum

386 neutralization. However, the structure to sequence pipeline was still successful in discovering FP-
387 specific mAbs without requiring expression and characterization of large panels of antibodies as
388 has historically been done, showcasing the power and efficiency of this tool for epitope specific
389 mAb isolation.

390 **Discussion**

391 In previous studies, NHPs immunized with HIV-1 Env soluble trimers with FP-proximal
392 N-linked glycans deleted elicited FP-directed responses [13,23]. Here, we report that having only one
393 of the four canonical FP glycans (ΔN241) absent does not robustly prime FP-targeting Abs in
394 NHPs. While the autologous BG505-CH505 immunizations primed low affinity and/or low
395 abundance C1/C2 and FP B cell populations, only upon heterologous boosting were significant
396 increases in C1/C2 and FP Abs observed via nsEMPEM and FP-ELISA titers, respectively.
397 Heterologous boosting induced weak neutralization breadth in one animal and high resolution
398 EMPEM analysis revealed a pAb that fully interacted with the FP. Our data supports previous
399 findings that autologous boosters bolster strain-specific responses rather than eliciting desired
400 cross-reactive immunity, which does occur with heterologous boosters[42,43,50,51].

401 The increased FP-directed responses observed after delivery of heterologous boosters is
402 unlikely to correlate with increased immunogenicity of the FP on the heterologous, AMC016
403 trimer. First, the FP motif in the BG505-CH505ΔN241, BG505-CH505+N241, and AMC016
404 immunogens are identical, an FP sequence grafted from BG505 (AVGIGAVF), as this is the most
405 commonly circulating FP sequence amongst HIV isolates (www.hiv.lanl.gov). Repeated
406 immunizations with BG505 SOSIP.664 trimer in rhesus macaques and rabbits also did not show
407 consistent elicitation of FP directed Abs[8,11,19,32,52,53], unless three or more glycans around the FP
408 were removed in the trimer immunogens[13,23]. Secondly, rabbits immunized with wild-type

409 AMC016 trimer, hence displaying the canonical FP sequence, AVGTIGAMF, did not elicit FP-
410 directed Abs, suggesting weak immunogenicity of AMC016 SOSIP trimer when fully
411 glycosylated[33]. Finally, the week 43 ELISA data suggest lack of FP recognition in the control
412 group after heterologous boosting, which indicates FP on the heterologous trimer is not uniquely
413 immunogenic in this study and did not prime a FP response.

414 Rather than priming a FP-directed response, the AMC016 immunogen boosted a small
415 population of B cells targeting the conserved FP and C1/C2 regions that had been primed by the
416 BG505-CH505ΔN241 or BG505-CH505+N241, respectively, in previous immunizations[54]. The
417 FP-ELISA showed significant difference in FP recognition in the polyclonal response after
418 heterologous boosting in the control group versus the experimental groups although both exhibit
419 FP-like responses via nsEMPEM after AMC016 immunizations (Fig 2 and S2). High resolution
420 cryoEMPEM reveals a newly characterized C1/C2 non-specific "FP" epitope in the control group
421 that does not engage with the FP itself but C1/C2 residues that are commonly observed in FP
422 specific epitopes as well[23]. The experimental group more consistently recognized the FP,
423 suggesting that while the FP priming was not robust, the lack of N241 glycan in the experimental
424 group priming immunogen did impact overall FP recognition in the immune response by the end
425 of the study.

426 Lack of robust FP priming by the chimeric antigens limited the recall response breadth
427 potential upon heterologous boosting [55–59]. In the absence of high-affinity Ab competition in the
428 serum, MBCs with moderate-to-low affinity for the boosting antigen can better form and populate
429 recall germinal centers to expand and evolve these low affinity and/or low abundance, cross-
430 reactive B cell clones with or without the occurrence of clonal bursts[42,45,54,60,61]. With little serum

431 Ab competition, the low abundance FP- and C1/C2-targeting MBCs produced by the chimeric
432 immunogens were able to engage the heterologous AMC016-based antigen. In some studies, the
433 recall response would include lower affinity and/or lower abundance MBCs, differentiating into
434 PCs to secrete Abs without further SHM, especially against heterologous viral variants[42,43,51,62].
435 Our results here indicate the preferential use of heterologous booster immunogens to focus the
436 immune system on epitopes of interest; however, further research needs to be done to boost GC
437 recall responses to drive iterative rounds of SHM to develop Ab breadth.

438 STS strategies were successful in pulling out epitope-specific monoclonal antibodies with
439 varying levels of FP engagement. While they proved to be non-neutralizing, the antibodies
440 constructed from our pAb EM map and sequencing data all recognized FP to different extents,
441 which is quite exciting and impressive when compared with the historically laborious antibody
442 discovery pipelines. More research has been done to improve the STS pipeline for improved
443 isolation for target-specific antibodies, which will help advance the speed for bnAb discovery and
444 target characterization as bnAbs are key for many vaccine efforts[63,64].

445 High-resolution EM analysis reveals on-target (FP) and off-target (base, V1V2V3, C3/V5,
446 and C1/C2 non-specific "FP") epitope details of humoral immune recognition. Glycan sub-
447 occupancy of the soluble trimer elicits off-target and distracting immune responses and more
448 studies need to be conducted to optimize glycan occupancy and homogeneity in vaccine
449 immunogens. The introduced disulfides at the base of the trimer, while unsuccessful in silencing
450 base responses, were efficient in mitigating in vivo trimer disassembly that had been seen in prior
451 soluble trimer immunizations[38]. The heterologous epitope boosting predictions would be a very
452 valuable tool for vaccine development, to allow for immunofocusing towards epitopes of interest
453 and away from immunogenic but nonprotective epitopes that consume valuable resources to elicit

454 non-neutralizing and nonprotective immune responses. However, for a boosting immunogen to be
455 successful, it will be imperative to design a priming immunogen strategy that strongly primes the
456 desired Ab responses.
457
458 **Methods**
459 **Immunogen and Probe Preparation**
460 All immunogens and soluble trimeric, Avi-tagged probes were produced in HEK293F
461 cells. Six days after transfection, the cell supernatants were harvested by centrifugation and
462 purified using *Galanthus nivalis* lectin (Vector Laboratories) affinity chromatography followed by
463 size exclusion chromatography (SEC) using a HiLoad 16/600 Superdex 200 pg (Cytiva) column.
464 Further purification was performed using two rounds of negative selection columns produced
465 using CNBr-activated Sepharose 4B beads (Cytiva) coupled to non-neutralizing mAbs according
466 to the manufacturer's instructions. First F105 negative selection was used to remove further
467 monomeric, dimeric, and non-closed-state-conformation trimeric protein species and
468 aggregates[65,66]. The unbound proteins, or closed state trimeric protein species or aggregates, in the
469 F105 column flow through were then applied to a second 19b negative selection column to remove
470 trimer species with a highly immunogenic conformation of the V3 glycan that leads to a lot of
471 strain specific neutralizing Ab responses[67]. The flow through of the 19b negative selection column
472 contained closed-state trimer protein species, which were then purified a second time using SEC.
473 Immunogen preps were tested for endotoxin using an Endosafe instrument (Charles River). Avi-
474 tagged proteins were then biotinylated following the manufacturer's protocol for BirA enzyme
475 (Avidity).
476

477 **Rhesus Macaques**

478 Twelve rhesus macaques (Macaca mulatta) of Indian origin were acquired and housed at
479 Emory National Primate Research Center and cared for according to NIH guidelines. Emory
480 University Institutional Animal Care and Use Committee [IACUC# 201800298] approved this
481 study. Animal care facilities are accredited by the U.S. Department of Agriculture (USDA) and
482 the Association for Assessment and Accreditation of Laboratory Animal Care (AAALAC)
483 International. Animals were treated with anesthesia (ketamine 5-10 mg/kg or telazol 3-6 mg/kg)
484 and analgesics for procedures such as osmotic pump implantation and removal, subcutaneous
485 immunization, blood draws, and lymph node fine needle aspirates as per veterinarian
486 recommendations and IACUC approved protocols. When osmotic pumps were implanted, animals
487 were kept in single, protected contact housing. At all other times, animals were kept in paired
488 housing. Rhesus macaques were male, an age range of 3-4 years old, and at the start of the study
489 a median weight of 5 kilograms. Animals were grouped to divide age, weight and gender as evenly
490 as possible between the two groups. After completion of the proposed study, animals were
491 transferred to other researchers upon the approval of the veterinarians.

492

493 **Animal Immunizations and sample collection**

494 Osmotic pumps (Alzet model 2004) were loaded with 50 μg soluble Env trimer immunogen
495 + 750 ug of SMNP Fig. 1B. Two pumps were subcutaneously (SC) implanted into each animal
496 (one pump each in the left and right mid-thighs). The immunogen/adjuvant mixture was secreted
497 continuously over the course of 4 weeks. The pumps were removed after 4 weeks. The animals
498 were boosted at three timepoints s.c. with a bolus injection of 100 ug soluble trimer immunogens
499 and 750 ug of SMNP (Figure 1) bilateral immunization split between the right and left mid- thigh.

500 Blood was collected at various time points into CPT tubes for PBMC and plasma isolation. Serum
501 was isolated using serum collection tubes and frozen. Plasma was used in ELISA and EMPEM
502 analysis. Serum was used for neutralization assays.
503
504 **FP-ELISA**
505 Streptavidin coated ELISA plates (Pierce Thermo Fisher), pre-blocked with BSA, were washed
506 with wash buffer (1X TBS, 0.1% BSA, 0.5% Tween-20) 3x before coating with biotinylated FP-
507 13 (InnoPep) (0.01 mg/mL in Wash Buffer) and left to rotate at 200 rpm and RT for two hours.
508 Then plates were washed 3x before 100 μL of polyclonal IgG (1 mg/mL) for each sample timepoint
509 or 100 μL RQk-FP mAbs 01-08 (150 μg/mL) was added to the plates and allowed to rotate at RT
510 for an hour. Plates were then washed 3x before adding secondary antibody conjugated to alkaline
511 phosphatase (AP) (anti-human Fab'2, goat antibody) and left to rotate for 30 minutes at RT. After
512 washing 3x, developing solution is applied and allowed to develop while rotating for 30 minutes
513 before stopping solution (2N NaOH) was used to stop the development. Plates were then read at
514 405 nm wavelength in a plate reader.
515
516 **Serum - ELISA**
517 Serum samples from animals were serially diluted (starting at 1:80) and plated on pre-coated wells
518 with BG505-CH505+N241 or AMC016 antigen or FP-13 (plates (Corning, Cat#: 3690) were
519 coated with Streptavidin (Invitrogen, Cat#: 434302), blocked with 2% BSA and then incubated
520 with biotinylated BG505-CH505+N241 or AMC016 or FP-13 probe). Env or FP binding-IgG
521 antibodies were detected using HRP goat anti-human IgG (Jackson ImmunoResearch, Cat#: 109-
522 035-098) and 1-Step™ Ultra TMB-ELISA Substrate Solution (Thermo Fisher Scientific, Cat#:

523 34029). The reaction was stopped with 2N of sulfuric acid (Ricca Chemical, Cat#: 8310-32) and
524 read at 450 nm on a FlexStation 3 plate reader (Molecular Devices).
525
526 **TZM-bl cell-based neutralization assay**
527 Env-pseudotyped virus neutralization assays completed at Duke were measured as a function of
528 reductions in luciferase (Luc) reporter gene expression after a single round of infection in TZM-
529 bl cells[68,69]. TZM-bl cells (also called JC57BL-13) were obtained from the NIH AIDS Research
530 and Reference Reagent Program, as contributed by John Kappes and Xiaoyun Wu. Briefly, a pre-
531 titrated dose of virus was incubated with serial dilutions of heat-inactivated (56 °C, 30 min) serum
532 samples in duplicate for 1 h at 37 °C in 96-well flat-bottom culture plates, followed by addition of
533 freshly trypsinized cells. One set of control wells received cells + virus (virus control) and another
534 set received cells only (background control). After 48 h of incubation, cells were lysed and
535 measured for luminescence using the Brit elite Luminescence Reporter Gene Assay System
536 (PerkinElmer Life Sciences). ID50/IC50 and ID80/IC80 neutralization titers/concentrations are
537 the dilution (serum/plasma samples) or concentration (mAbs) at which relative luminescence units
538 (RLU) were reduced by 50% or 80% compared to virus control wells after subtraction of
539 background RLUs from cells controls.
540
541 **FP Competition Neutralization Assay**
542 TZM-bl neutralization assay using pseudoviruses CH505TF and BG505/T332N.N611A.
543 Serum sample were titrated with or without FP-10, with a starting serum dilution of 1:20 and FP-
544 10 concentration of 50 ng/mL; followed by 3-fold serial dilution for 8 total dilutions. VRC34.01
545 was titrated with or without FP-10, with a start concentration of 5 μg/mL and FP-10 concentration

546 of 50 ng/mL; followed by 3-fold serial dilution for 8 total dilutions. Peptide and serum/mAb
547 mixture were incubated at 37'C for 1 hr before viruses were added for routine neutralization assay.
548 Cytotoxicity was observed in all wells with 50 ng/mL peptide (first dilution/concentration for
549 serum/mAb titration). Serum dilution 1:10 and VRC34.01 concentration of 5 μg/mL were
550 excluded from all assays for data analysis.
551
552 **LN-FNA and Cell Sorting**
553 Lymph node fine needle aspirates were collected and processed as previously described[24].
554 B cells probes were prepared for flow cytometry by premixing individual probes with
555 fluorochrome-conjugated streptavidin Ax647, BV421, or BV650 at RT for 20 minutes.
556 For the FNA phenotyping panel, cells were incubated with appropriate conjugated probes in a
557 stepwise fashion for 20 minutes at 4C. Following probe addition and incubation, surface antibodies
558 (Table S12) were added directly to the cells and incubated for 30 minutes at 4C. Cells were washed
559 twice, fixed for 30 minutes with 1% PFA at 4C, washed twice again, and acquired. Representative
560 gating as well as antibody and clones for GC B cell and GC TFH cell flow cytometry is provided
561 (Fig S2).
562 For the 10X B cell sorting panel, cells were incubated with appropriate conjugated probes for 30
563 minutes at 4C. Following probe addition and incubation, surface antibodies (Table S13) and
564 appropriate TotalSeq cell hashing antibody were added directly to the cells and incubated for 30
565 minutes at 4C. Cells were then washed twice and acquired.
566
567 **Bulk B cell receptor sequencing**

568 Total RNA was extracted from cryo-preserved peripheral blood mononuclear cells (PBMCs) of
569 non-human primates (NHP) using the Qiagen RNeasy Kit (Catalog No. 75144), following the
570 manufacturer's protocol. The extracted RNA served as the template for reverse transcription,
571 which was conducted using the Superscript IV Reverse Transcriptase and specific primers
572 targeting the constant region of immunoglobulin heavy chains (IgM, IgG) and light chains (IgK,
573 IgL) of *Macaca mulatta*. The cDNA was then subjected to a two-step PCR amplification process.
574 In the first step, primers specific to the V-gene regions were used to amplify the target sequences.
575 In the second step, the amplified products were further processed to include Illumina adapters
576 necessary for high-throughput sequencing. The library preparation and PCR protocols were
577 adapted from the methods described by Briney et al., 2019. Sequencing was performed on an
578 Illumina NovaSeq 6000 platform using a paired-end 2x251 bp cycle run. The raw sequencing data
579 was processed using abstar, which employed sequence merging, alignment, and annotation,
580 producing a JSON-formatted output. The reference database used in the analysis contained unique
581 amino acid sequences corresponding to the VDJ regions of heavy and light chain antibodies.
582
583 **nsEMPEM**
584 Plasma samples were heat inactivated for 1 hour at 56C for live virus before purification via
585 PrismA affinity column to isolate pAbs. pAbs were then digested to generate polyclonal fAbs with
586 papain[70]. Once clean fabs were isolated, 500 ug of polyclonal fab were left to complexed with 15
587 ug of probing immunogen overnight at RT. Samples were then SEC purified to isolate trimer-fab
588 complexes. After complex isolation, samples were stained and imaged on a FEI Talos microscope
589 at a 73,000x magnification using Leginon. Relion v3.0 was used for 2D classification, 3D

590 classification and 3D refinement. UCSF Chimera[71] and Segger[72] were used for visualizing and
591 segmenting the EM density maps, respectively.
592
593 **CryoEMPEM sample preparation and imaging**
594 ~10 mg of clean, polyclonal fab sample was complexed with 250 ug of probing trimer and left to
595 complex overnight at RT. Samples were then SEC purified and the fab-trimer complexes were
596 isolated. Samples were concentrated to 5-7 mg/ml. Just before sample application, samples were
597 combined with lauryl maltose neopentyl glycol (LMNG) to a final concentration of 0.005. Samples
598 were then vitrified using a Vitrobot mark IV (Thermo Fisher Scientific) on Quantifoil Cu 1.2/1.3
599 300C-mesh grids (Electron Microscopy Sciences) with 5-7 second blot times with a chamber set
600 to 10C. Data collection for RUu18 week 14 was done on a 200 kV Talos Arctica and a K2 summit
601 direct electron detector camera. Data collection for RQk18 week 43 was done on a 300 kV Titan
602 Krios with a K2 summit direct electron detector camera.
603
604 **CryoEMPEM processing**
605 CryoEMPEM was performed according to protocols previously described[26]. Micrograph movie
606 frame alignments and dose-weighting was done through MotionCor2[73]. Data was processed using
607 cryoSPARCv3.2.0[74] and GCTF was used for CTF parameter estimation[75]. In cryosparc, template
608 picker was used to pick trimer-fab complexes before running the particles through two rounds of
609 2D classification. Clean particles were selected for 3D homogenous refinement in C1 and C3
610 symmetries. Particles were then symmetry expanded for focused classification. In UCSF chimera,
611 a 40 A mask was placed around 3 epitopes: FP, V1V2V3 and the Base. Symmetry expanded
612 particles, with the C3 symmetry map and aligned sphere masks were used as inputs for 3D

613 variability, done for each epitope investigated. Data processing for the different epitopes at this
614 point were done separately but in parallel. Particles showing epitopes of interest were grouped and
615 run through non-uniform refinement to obtain the high-resolution maps used for interpretation (Fig
616 S3).
617

618 **CryoEMPEM model-building**

619 An unliganded BG505 SOSIP (PDB 6V0R) was initially docked into each refined map in UCSF
620 Chimera. Then, MODELLER was used to change the docked Env sequence to the autologous and
621 heterologous boosts, for their respective data sets[76]. We docked polyalanine Fab models with
622 fiducial markers (conserved disulfides and IMGT anchor residues) into each map and assigned the
623 heavy and light chain orientations based on conformations of the FR2 and FR3 regions as well as
624 CDR3 lengths. CDR lengths were determined and adjusted during manual model building using
625 Coot[77,78]. Entire complexes were refined using both Rosetta[79] and Phenix[80,81].
626

627 **Structure to sequence**

628 Structure to sequence predictions were done as previously described[49]. Inferred sequences were
629 then searched within the B cell sequence library described above, which was incorporated into a
630 Jupyter Notebook (www.jupyter.com) environment. Top hits were verified against the cryo-EM
631 map to converge the pAb phenotype with the verified sequences. MolProbity[82] and EMRinger[83]
632 were used to evaluate the final models before they were deposited to the PDB with polyalanine
633 fab models representing the pAb Fv.
634

635 **Data Availability**

636 CryoEMPEM densities and structures were deposited to the protein Data Bank (PDB) with the
637 following accession codes: 9NHH, 9NHI, 9NHJ, 9NI9, 9NHK, 9NHL, 9NHM, 9NHN, 9NHO,
638 and Electron Microscopy Data Bank (EMDB) with the following accession codes: EMD-49411 to
639 EMD-49418, EMD-49457, and (FP-mAb05). Negative maps were deposited to EMDB with the
640 following accession numbers: EMD-70702 - EMD-70717. Entries with polyclonal fab in complex
641 with BG505-CH505ΔN241 are reported as BG505-CH505d241 due to character limitations for
642 EMDB and PDB depositions.
643

644 **Acknowledgements**

645 The authors thank Hannah L. Turner, Charles A. Bowman, Jean-Christophe Ducom, Bill
646 Anderson, William Lessin and Anant Gharpure (The Scripps Research Institute) for electron
647 microscopy, data acquisition and processing help. The authors also acknowledge Drs. Hailee
648 Perrett and Lauren Holden for their help in manuscript preparation. This research was supported
649 partly by the National Institute of Allergy and Infectious Disease of the National Institutes of
650 Health Award Numbers AI145629 and AI136621. This work was funded by Cooperative
651 Agreement award UM1 AI144462 in partnership with the Division of AIDS, NIAID. This research
652 was funded in part by the Emory National Primate Research Center Grant Nos. ORIP/OD
653 P51OD011132 and U42 PDP11023. The Emory National Primate Center is supported by the
654 National Institutes of Health, Office of Research Infrastructure Programs/OD [P51OD011132 and
655 U42 PDP11023] The authors are responsible for the contents of this manuscript, which do not
656 necessarily represent the views of the US Government nor NIAID. The funders participated in no
657 role of the study design, decisions, investigation, and preparation or publishing of this manuscript.
658

Competing Interests

The authors declare no competing interests.

Author Contributions

P.P.P. – Conceptualization, Data curation, Formal Analysis, Investigation, Methodology, Validation, Visualization, Writing – original draft, Writing – review & editing. C.A.C. – Conceptualization, Data curation, Formal Analysis, Investigation, Methodology, Validation, Writing – review and editing. J.Q. – Data curation, Formal Analysis, Investigation, Visualization, Writing – review & editing. D.G.C. – Resources, Writing – review & editing. D.B. – Formal Analysis, Writing – review & editing. A.S.T. – Investigation. C.A.E. – Resources. J.T.N. – Resources. S.T.R. – Investigation. H.G. – Investigation, Resources, Writing – review & editing. X.S. – Investigation, Resources, Writing – review & editing. K.M.G. – Investigation, Resources. J.H. – Investigation, Resources, Writing – review & editing. K.K.M. – Investigation, Resources, Writing – review & editing. E.B.A. – Resources. A.L. – Investigation, Resources, M.B.M. – Investigation, Resources, J.D.A. – Formal Analysis, Investigation, Visualization, Writing – review and editing. G.O. – Formal Analysis, Supervision. B.B. – Resources. M.C. – Resources. D.M. – Resources. G.S. – Resources. D.J.I. – Resources. S.C. – Conceptualization, Funding Acquisition, Project Administration, Resources, Supervision, Writing – review and editing. A.B.W. – Conceptualization, Funding Acquisition, Project Administration, Resources, Supervision, Writing – review & editing.

680 **Figures**
681
682

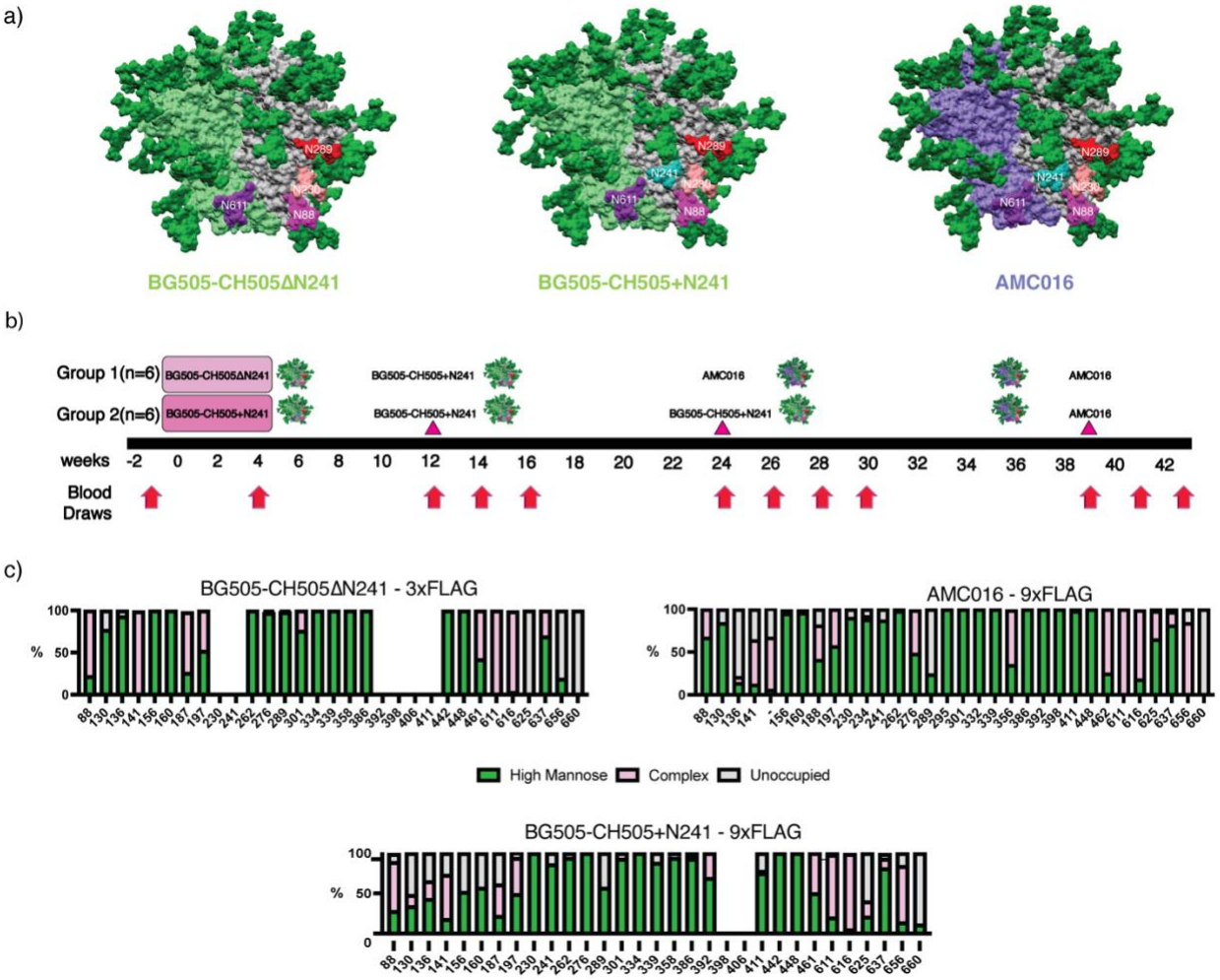

683
684
685 **Figure 1. FP targeting Immunogens and Immunizations.**

686 a) Surface representations for BG505-CH505ΔN241 and BG505-CH505+N241, which are
687 BG505 (Clade A)/CH505 (Clade C) chimeric trimers. The AMC016 trimer is a Clade B
688 isolate. FP glycans are depicted as follows: N88 glycan in magenta, N230 glycan in
689 salmon, N241 glycan in turquoise, and N611 glycan in purple. The N289 glycan is
690 depicted in red.
691 b) Immunization schedule. Osmotic pump immunogen delivery period is shaded in pink.
692 Bolus immunizations are depicted with triangle indicator.
693 c) Glycan Analysis of immunogens used in this study and impacts of Flag tag length on
694 glycan occupancy.
695
696
697

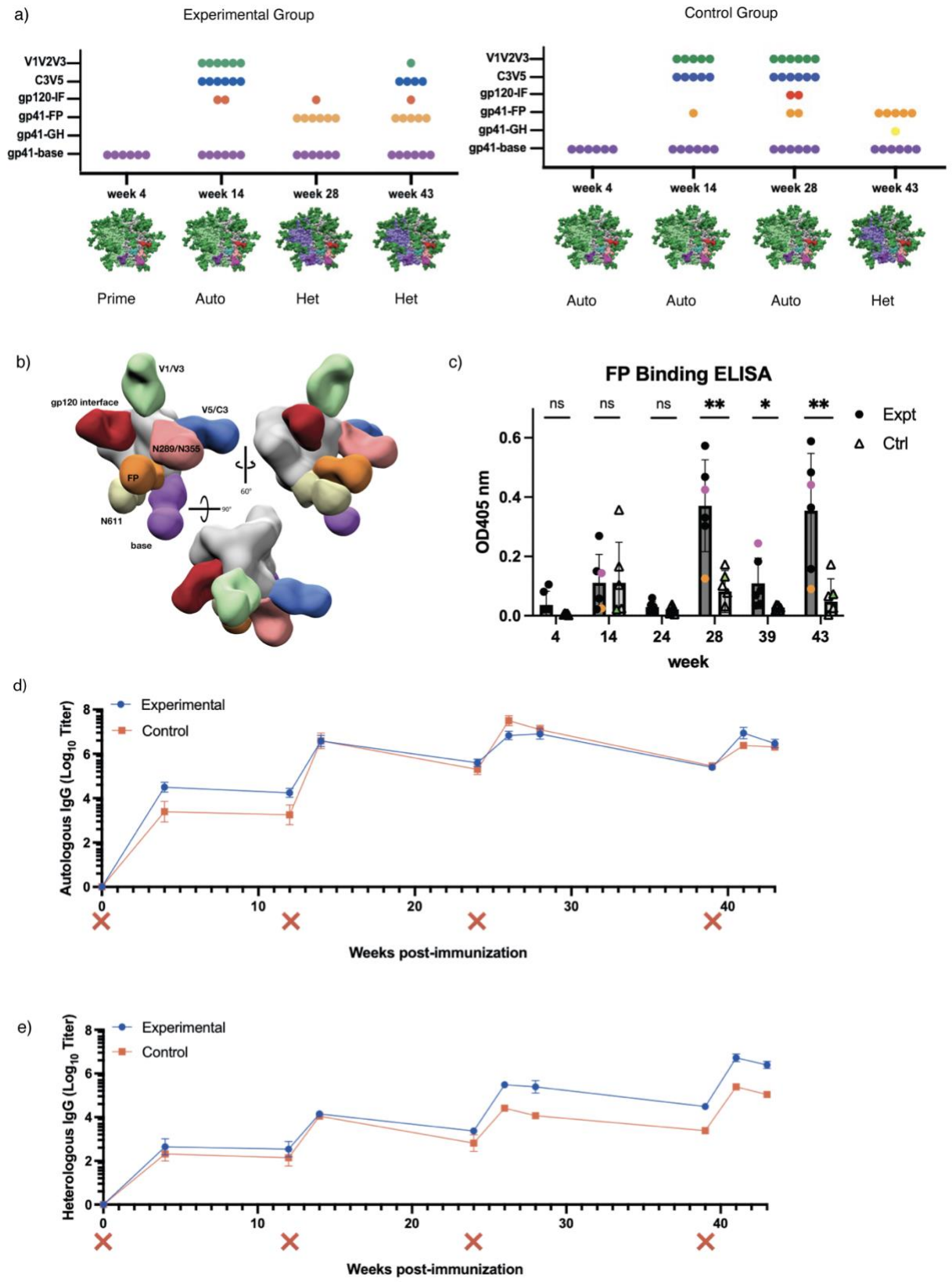

Figure 2. Humoral response analysis via ELISA and nsEMPEM

a) nsEMPEM dot plot results after each immunization

701 b) EMPEM figure legend from multiple views
702 c) FP-ELISA binding for time points also analyzed via nsEMPEM – experimental group (dark
703 grey) versus control group (light grey). Animals RUu18, RQk18, and LJ66 are highlighted
704 in green, pink and orange, respectively.
705 d) Autologous trimer ELISA showing serum recognition of BG505-CH505+N241 trimer from
706 control group (red) as well as experimental group (blue). (X) mark indicates
707 immunization
708 e) Heterologous trimer ELISA showing serum recognition of Heterologous AMC016 trimer
709 from control group (red) as well as experimental group (blue)
710

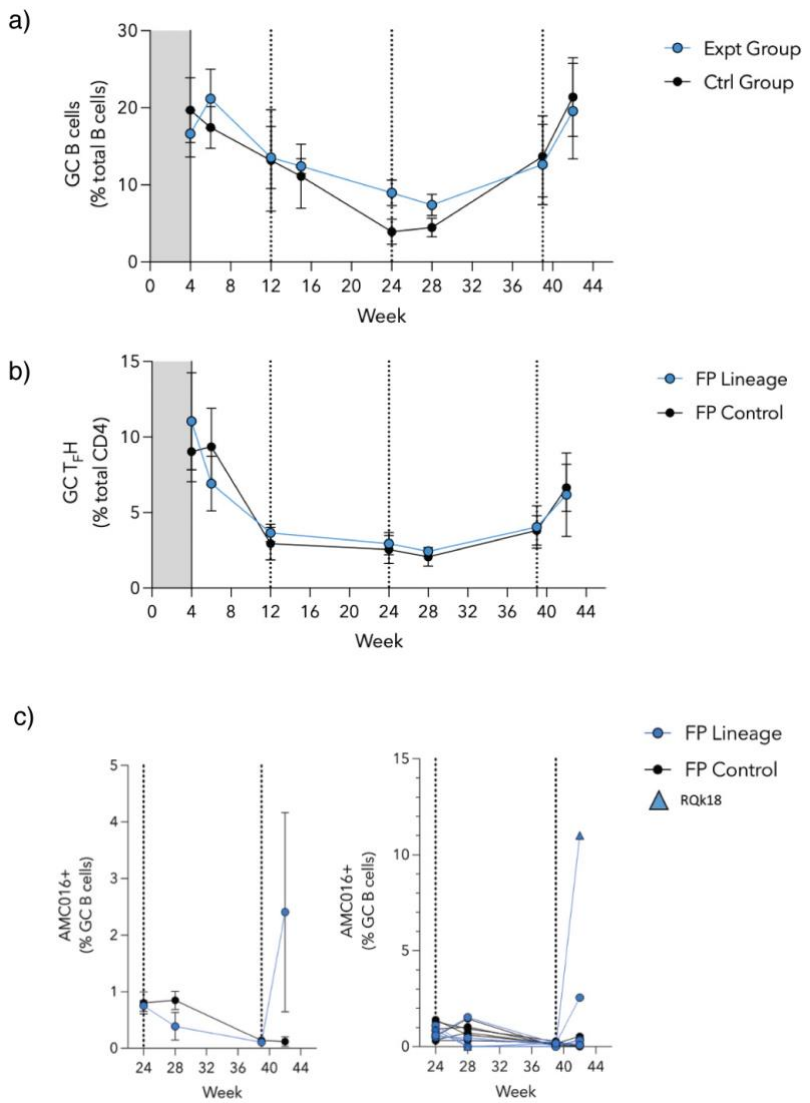

Figure 3. Flow cytometry reveals limited changes in GC B and TFH cell populations

a) Quantification of GC B cell kinetics as a percentage of total CD20+ B cells. Experimental group shown in blue circles while control group are shown in black circles.
b) Quantification of GC Tfh cell kinetics as a percentage of total CD4+ T cells.
c) % GC B cells that are AMC016+ following the boosts at weeks 24 and 39. Individual animals are shown on the graph to the right with animal RQk18 being the highest binder of the experimental group (depicted as a blue triangle).

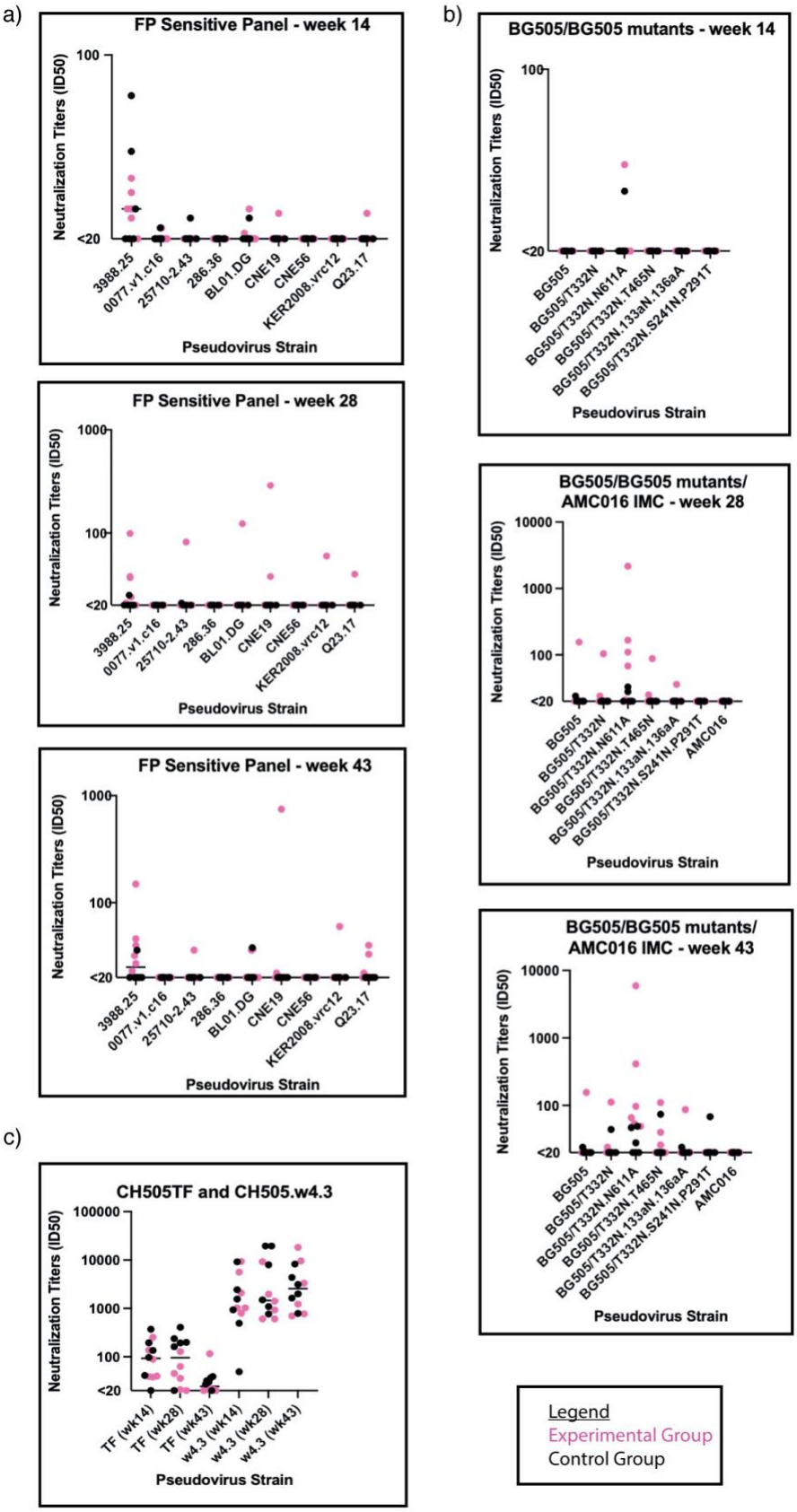
a)
FP Sensitive Panel - week 14
Neutralization Titers (ID50)
100
<20
3988.25
0077.v1.c16
25710-2.43
286.36
BL01.DG
CNE19
CNE56
KER2008.vrc12
Q23.17
Pseudovirus Strain
FP Sensitive Panel - week 28
1000
100
<20
FP Sensitive Panel - week 43
b)
BG505/BG505 mutants - week 14
BG505
BG505/T332N
BG505/T332N.N611A
BG505/T332N.T465N
BG505/T332N.133aN.136aA
BG505/T332N.S241N.P291T
BG505/BG505 mutants/
AMC016 IMC - week 28
10000
AMC016
BG505/BG505 mutants/
AMC016 IMC - week 43
c)
CH505TF and CH505.w4.3
100000
TF (wk14)
TF (wk28)
TF (wk43)
w4.3 (wk14)
w4.3 (wk28)
w4.3 (wk43)
Legend
Experimental Group
Control Group

719

720 **Figure 4. Serum neutralization sporadically observed after heterologous boosting**

721 a) Comparison of FP-Sensitive pseudovirus panel serum neutralization between weeks
722 14 (top), 28 (middle), and 43 (bottom). (Experimental group is shown in magenta
723 circles and the control group in black circles). Y-axis is in log scale.
724 b) Comparison of BG505 pseudovirus panel serum neutralization between weeks 14
725 (top), 28 (middle), 43 (bottom). Y-axis is in log scale.
726 c) Comparison of CH505 pseudovirus panel serum neutralization. Y-axis is in log scale.
727
728

729

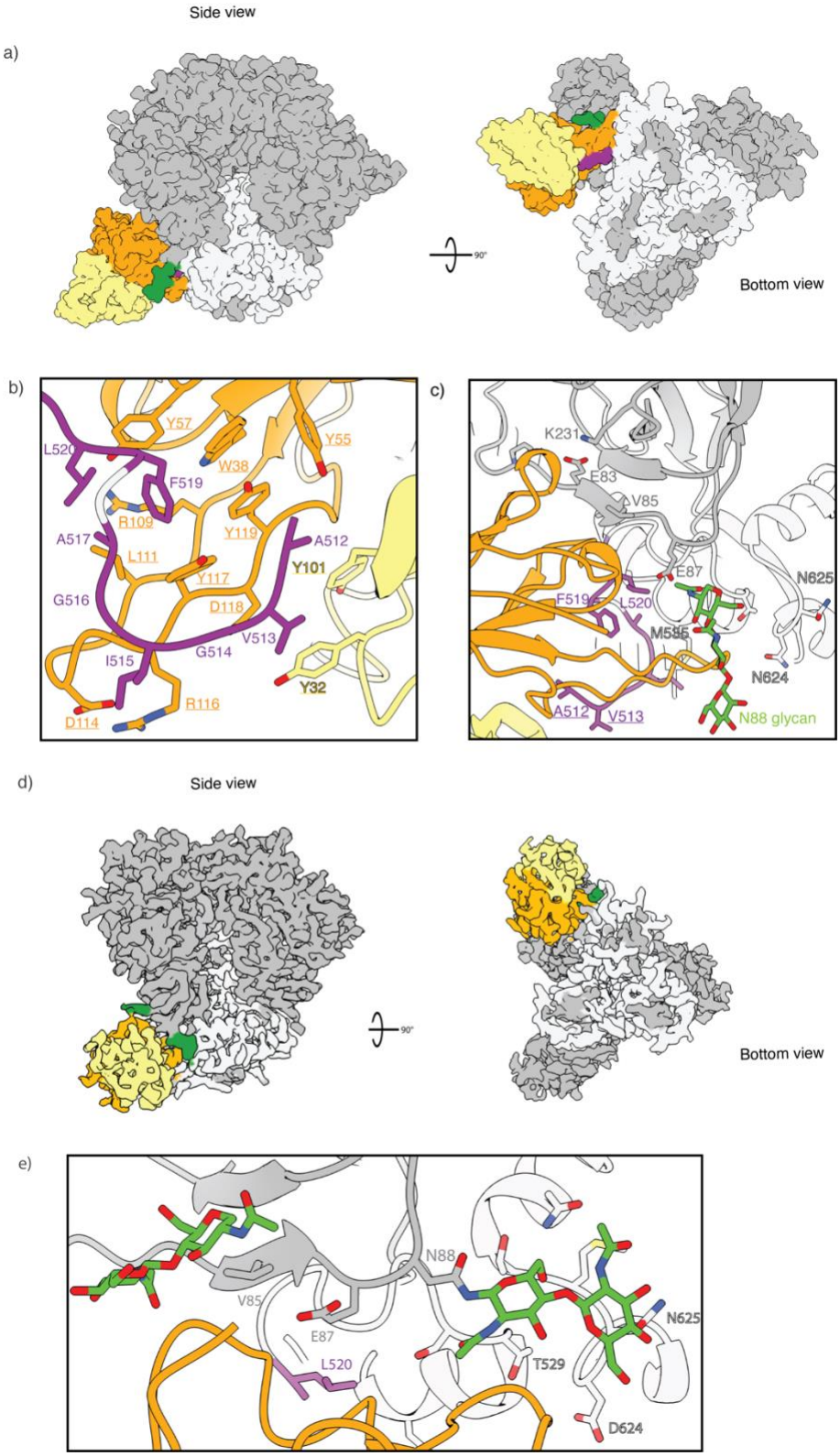

730

731 **Figure 5. FP-targeting versus FP-proximal immune responses share overlapping epitopes**

a) RQk-FP-A pAb1 from week 43 in complex with Heterologous Boost (left panel– side view; right panel – bottom view). The heavy chain (HC) is depicted in orange while the light chain (LC) is shown in yellow. The FP is shown in purple, the N88 glycan in green, gp120 subunit in grey and the gp41 subunit in white.
b) RQk-FP-A pAb inferred hydrophobic and aromatic residues along its HCDR3 and LCDR1 and LCDR3 form a hydrophobic pocket that stabilizes the N-terminus of the FP
c) RQk-FP-A pAb interacts with the N88 glycan and C1/C2 beta strands as well as the HR2 domain of gp41.
d) RUu-FP-1 cryoEM map (Left – bottom view; right – side view)
e) RUu-FP-1 pAb makes contacts with the C1 beta strand, HR2 and canonical FP glycans N241 and N88

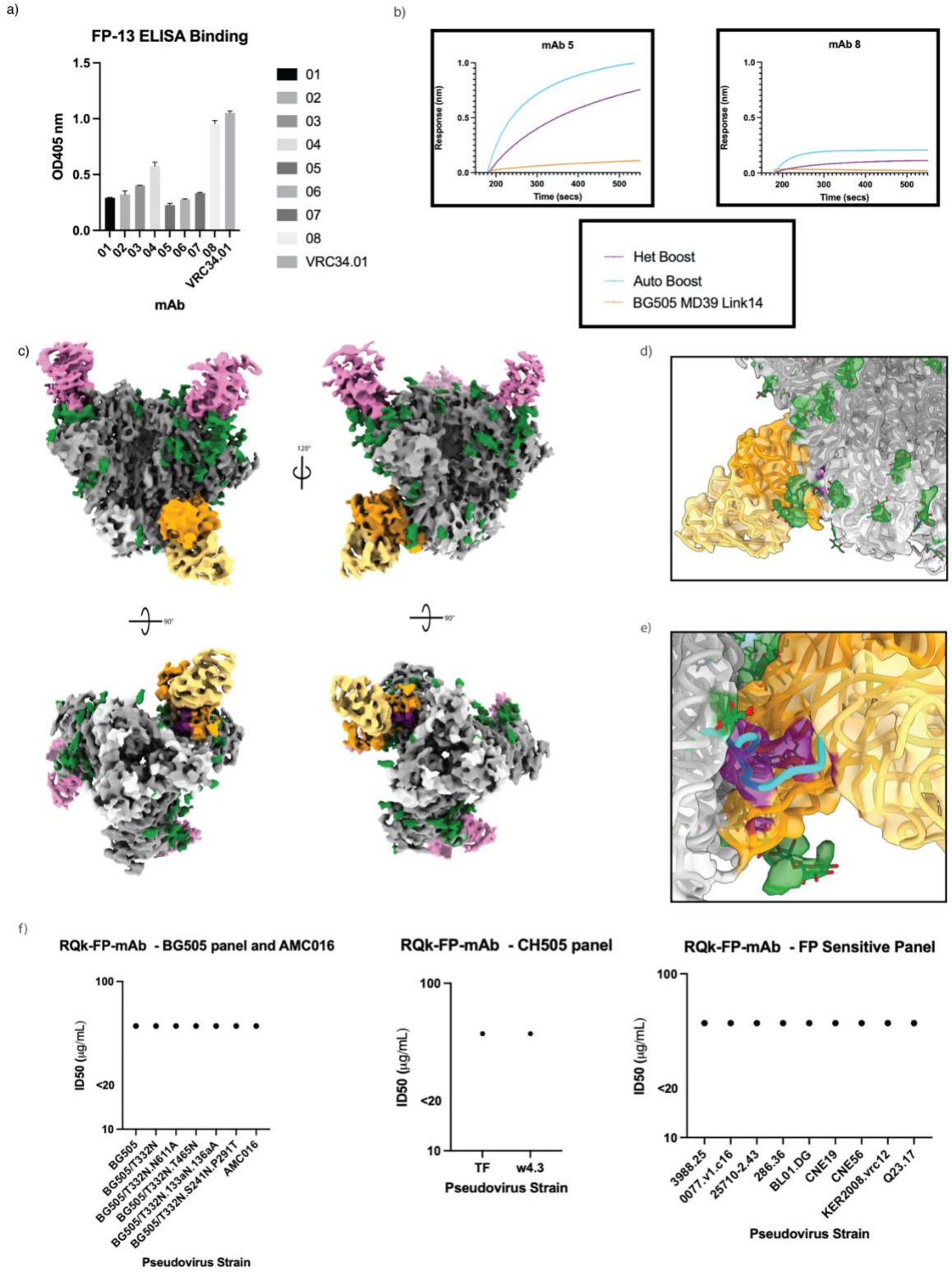

Figure 6. STS solves mAbs that bind to the FP region with varying FP interactions

a) FP-ELISA showcasing degree of FP interaction of the 8 different FP mAbs expressed from STS

751 b) BLI curves of mAbs 05 (left) and 08 (right) interacting with trimers AMC016 (purple),
752 BG505-CH505+N241 (blue) and negative control BG505 MD39 link 14 (orange)
753 c) Colored EM maps of AMC016 (gp120 – dark gray, gp41 – light gray, glycans – green) in
754 complex with RQk-FP-mAb 05 (heavy chain – orange, light chain – pale yellow), and
755 PGT122 (pink). Bottom views showcase FP in purple.
756 d) RQk-FPA pAb model, when docked into the mAb 05 EM map, shows high degree of
757 overlap of FP antibody and FP density, shows same angle of approach and N88 glycan
758 interactions
759 e) RQk-FPA pAb modelled FP regions (blue) shows poor overlap with mAb 05 EM map
760 density for FP region (purple), showing slightly different modes of FP engagement
761 between the two antibodies
762 f) Antibody neutralization panel of RQk-FP mAbs 01, 03, 05, and 07 show >50.00 μg/mL
763 concentration for PV neutralization, which is interpreted as non-neutralizing. PV panels
764 include BG505 and related mutants panel and AMC016 (right), a CH505 PV panel
765 (middle) and a FP-sensitive PV panel (right)
766
767
768
769 **References**

770

771 1. Klein F, Diskin R, Scheid JF, et al. Somatic mutations of the immunoglobulin framework are
772 generally required for broad and potent HIV-1 neutralization. *Cell*. 2013;153(1):126-138.
773 doi:10.1016/j.cell.2013.03.018

774 2. Klasse PJ, Ozorowski G, Sanders RW, Moore JP. Env Exceptionalism: Why Are HIV-1 Env
775 Glycoproteins Atypical Immunogens? *Cell Host and Microbe*. 2020;27(4):507-518.
776 doi:10.1016/j.chom.2020.03.018

777 3. Kepler TB, Wiehe K. Genetic and structural analyses of affinity maturation in the humoral
778 response to HIV-1. *Immunological Reviews*. 2017;275(1):129-144. doi:10.1111/imr.12513

779 4. Wyatt R, Sodroski J. The HIV-1 envelope glycoproteins: fusogens, antigens, and immunogens.
780 *Science*. 1998;280(5371):1884-1888. doi:10.1126/science.280.5371.1884

781 5. Eckert DM, Kim PS. Mechanisms of viral membrane fusion and its inhibition. *Annu Rev*
782 *Biochem*. 2001;70:777-810. doi:10.1146/annurev.biochem.70.1.777

783 6. Sanders RW, Vesanen M, Schuelke N, et al. Stabilization of the soluble, cleaved, trimeric form
784 of the envelope glycoprotein complex of human immunodeficiency virus type 1. *J Virol*.
785 2002;76(17):8875-8889. doi:10.1128/jvi.76.17.8875-8889.2002

786 7. Sanders RW, Moore JP. Native-like Env trimers as a platform for HIV-1 vaccine design.
787 *Immunol Rev*. 2017;275(1):161-182. doi:10.1111/imr.12481

788 8. Sanders RW, van Gils MJ, Derking R, et al. HIV-1 VACCINES. HIV-1 neutralizing antibodies
789 induced by native-like envelope trimers. *Science*. 2015;349(6244):aac4223.
790 doi:10.1126/science.aac4223

791 9. Chen B. Molecular Mechanism of HIV-1 Entry. *Trends in Microbiology*. 2019;27(10):878-891.
792 doi:10.1016/j.tim.2019.06.002

793 10. Xu K, Acharya P, Kong R, et al. Epitope-based vaccine design yields fusion peptide-
794 directed antibodies that neutralize diverse strains of HIV-1. *Nat Med*. 2018;24(6):857-867.
795 doi:10.1038/s41591-018-0042-6

796 11. Kong R, Xu K, Zhou T, et al. Fusion peptide of HIV-1 as a site of vulnerability to
797 neutralizing antibody. *Science*. 2016;352(6287):828-833. doi:10.1126/science.aae0474

798 12. Cottrell CA, van Schooten J, Bowman CA, et al. Mapping the immunogenic landscape of
799 near-native HIV-1 envelope trimers in non-human primates. *PLoS Pathog*.
800 2020;16(8):e1008753. doi:10.1371/journal.ppat.1008753

801 13. Cheng C, Duan H, Xu K, et al. Immune Monitoring Reveals Fusion Peptide Priming to
802 Imprint Cross-Clade HIV-Neutralizing Responses with a Characteristic Early B Cell Signature.
803 *Cell Reports*. 2020;32(5). doi:10.1016/j.celrep.2020.107981

804 14. Ou L, Kong WP, Chuang GY, et al. Preclinical Development of a Fusion Peptide Conjugate
805 as an HIV Vaccine Immunogen. *Scientific Reports*. 2020;10(1). doi:10.1038/s41598-020-
806 59711-y

807 15. Sastry M, Changela A, Gorman J, et al. Diverse Murine Vaccinations Reveal Distinct
808 Antibody Classes to Target Fusion Peptide and Variation in Peptide Length to Improve HIV
809 Neutralization. *J Virol*. Published online April 26, 2023:e0160422. doi:10.1128/jvi.01604-22

810 16. Blattner C, Lee JH, Sliepen K, et al. Structural delineation of a quaternary, cleavage-
811 dependent epitope at the gp41-gp120 interface on intact HIV-1 Env trimers. *Immunity*.
812 2014;40(5):669-680. doi:10.1016/j.immuni.2014.04.008

813 17. Lee JH, Ozorowski G, Ward AB. Cryo-EM structure of a native, fully glycosylated, cleaved
814 HIV-1 envelope trimer. *Science*. 2016;351(6277):1043-1048. doi:10.1126/science.aad2450

815 18. van Gils MJ, van den Kerkhof TLGM, Ozorowski G, et al. An HIV-1 antibody from an elite
816 neutralizer implicates the fusion peptide as a site of vulnerability. *Nat Microbiol*.
817 2016;2:16199. doi:10.1038/nmicrobiol.2016.199

818 19. Klasse PJ, Ketas TJ, Cottrell CA, et al. Epitopes for neutralizing antibodies induced by HIV-
819 1 envelope glycoprotein BG505 SOSIP trimers in rabbits and macaques. *PLoS Pathog*.
820 2018;14(2):e1006913. doi:10.1371/journal.ppat.1006913

821 20. Pauthner M, Havenar-Daughton C, Sok D, et al. Elicitation of Robust Tier 2 Neutralizing
822 Antibody Responses in Nonhuman Primates by HIV Envelope Trimer Immunization Using
823 Optimized Approaches. *Immunity*. 2017;46(6):1073-1088.e6.
824 doi:10.1016/j.immuni.2017.05.007

825 21. Pegu A, Lovelace SE, DeMouth ME, et al. Antibodies targeting the fusion peptide on the
826 HIV envelope provide protection to rhesus macaques against mucosal SHIV challenge. *Sci*
827 *Transl Med*. 2024;16(730):eadh9039. doi:10.1126/scitranslmed.adh9039

828 22. Wang H, Cheng C, Dal Santo JL, et al. Potent and broad HIV-1 neutralization in fusion
829 peptide-primed SHIV-infected macaques. *Cell*. doi:10.1016/j.cell.2024.10.003

830 23. Cottrell CA, Pratap PP, Cirelli KM, et al. Priming antibody responses to the fusion peptide
831 in rhesus macaques. *NPJ Vaccines*. 2024;9(1):126. doi:10.1038/s41541-024-00918-9

832 24. Cirelli KM, Carnathan DG, Nogal B, et al. Slow Delivery Immunization Enhances HIV
833 Neutralizing Antibody and Germinal Center Responses via Modulation of
834 Immunodominance. *Cell*. 2019;177(5):1153-1171.e28. doi:10.1016/j.cell.2019.04.012

835 25. Bianchi M, Turner HL, Nogal B, et al. Electron-Microscopy-Based Epitope Mapping
836 Defines Specificities of Polyclonal Antibodies Elicited during HIV-1 BG505 Envelope Trimer
837 Immunization. *Immunity*. 2018;49(2):288-300.e8. doi:10.1016/j.immuni.2018.07.009

838 26. Antanasijevic A, Sewall LM, Cottrell CA, et al. Polyclonal antibody responses to HIV Env
839 immunogens resolved using cryoEM. *Nat Commun*. 2021;12(1):4817. doi:10.1038/s41467-
840 021-25087-4

841 27. Liao HX, Lynch R, Zhou T, et al. Co-evolution of a broadly neutralizing HIV-1 antibody and
842 founder virus. *Nature*. 2013;496(7446):469-476. doi:10.1038/nature12053

843 28. Sanders RW, Derking R, Cupo A, et al. A next-generation cleaved, soluble HIV-1 Env
844 trimer, BG505 SOSIP.664 gp140, expresses multiple epitopes for broadly neutralizing but not
845 non-neutralizing antibodies. *PLoS Pathog*. 2013;9(9):e1003618.
846 doi:10.1371/journal.ppat.1003618

847 29. McCoy LE, van Gils MJ, Ozorowski G, et al. Holes in the Glycan Shield of the Native HIV
848 Envelope Are a Target of Trimer-Elicited Neutralizing Antibodies. *Cell Reports*.
849 2016;16(9):2327-2338. doi:10.1016/j.celrep.2016.07.074

850 30. Silva M, Kato Y, Melo MB, et al. A particulate saponin/TLR agonist vaccine adjuvant
851 alters lymph flow and modulates adaptive immunity. *Sci Immunol*. 2021;6(66):eabf1152.
852 doi:10.1126/sciimmunol.abf1152

853 31. van Haaren MM, McCoy LE, Torres JL, et al. Antibodies from Rabbits Immunized with
854 HIV-1 Clade B SOSIP Trimers Can Neutralize Multiple Clade B Viruses by Destabilizing the
855 Envelope Glycoprotein. *Journal of Virology*. 2021;95(17). doi:10.1128/jvi.00094-21

856 32. Yang YR, McCoy LE, van Gils MJ, et al. Autologous Antibody Responses to an HIV
857 Envelope Glycan Hole Are Not Easily Broadened in Rabbits. *J Virol*. 2020;94(7):e01861-19.
858 doi:10.1128/JVI.01861-19

859 33. Schorcht A, Cottrell CA, Pugach P, et al. The Glycan Hole Area of HIV-1 Envelope Trimers
860 Contributes Prominently to the Induction of Autologous Neutralization. *J Virol*.
861 2022;96(1):e0155221. doi:10.1128/JVI.01552-21

862 34. Behrens AJ, Crispin M. Structural principles controlling HIV envelope glycosylation.
863 *Current Opinion in Structural Biology*. 2017;44:125-133. doi:10.1016/j.sbi.2017.03.008

864 35. Cao L, Pauthner M, Andrabi R, et al. Differential processing of HIV envelope glycans on
865 the virus and soluble recombinant trimer. *Nat Commun*. 2018;9(1):3693.
866 doi:10.1038/s41467-018-06121-4

867 36. Binley JM, Sanders RW, Master A, et al. Enhancing the proteolytic maturation of human
868 immunodeficiency virus type 1 envelope glycoproteins. *J Virol*. 2002;76(6):2606-2616.
869 doi:10.1128/jvi.76.6.2606-2616.2002

870 37. Derking R, Allen JD, Cottrell CA, et al. Enhancing glycan occupancy of soluble HIV-1
871 envelope trimers to mimic the native viral spike. *Cell Rep*. 2021;35(1):108933.
872 doi:10.1016/j.celrep.2021.108933

873 38. Turner HL, Andrabi R, Cottrell CA, et al. Disassembly of HIV envelope glycoprotein trimer
874 immunogens is driven by antibodies elicited via immunization. *Sci Adv*. 2021;7(31):eabh2791.
875 doi:10.1126/sciadv.abh2791

876 39. Yang L, Sharma SK, Cottrell C, et al. Structure-Guided Redesign Improves NFL HIV Env
877 Trimer Integrity and Identifies an Inter-Protomer Disulfide Permitting Post-Expression
878 Cleavage. *Front Immunol*. 2018;9:1631. doi:10.3389/fimmu.2018.01631

879 40. Nogal B, Bianchi M, Cottrell CA, et al. Mapping Polyclonal Antibody Responses in Non-
880 human Primates Vaccinated with HIV Env Trimer Subunit Vaccines. *Cell Reports*.
881 2020;30(11):3755-3765.e7. doi:10.1016/j.celrep.2020.02.061

882 41. Hu JK, Crampton JC, Cupo A, et al. Murine Antibody Responses to Cleaved Soluble HIV-1
883 Envelope Trimers Are Highly Restricted in Specificity. *J Virol*. 2015;89(20):10383-10398.
884 doi:10.1128/JVI.01653-15

885 42. Wong R, Belk JA, Govero J, et al. Affinity-Restricted Memory B Cells Dominate Recall
886 Responses to Heterologous Flaviviruses. *Immunity*. 2020;53(5):1078-1094.e7.
887 doi:10.1016/j.immuni.2020.09.001

888 43. Leach S, Shinnakasu R, Adachi Y, et al. Requirement for memory B-cell activation in
889 protection from heterologous influenza virus reinfection. *Int Immunol*. 2019;31(12):771-779.
890 doi:10.1093/intimm/dxz049

891 44. Torrents de la Peña A, Sewall LM, de Paiva Froes Rocha R, et al. Increasing sensitivity of
892 antibody-antigen interactions using photo-cross-linking. *Cell Rep Methods*.
893 2023;3(6):100509. doi:10.1016/j.crmeth.2023.100509

894 45. Victora GD, Nussenzweig MC. Germinal Centers. *Annu Rev Immunol*. 2022;40(1):413-
895 442. doi:10.1146/annurev-immunol-120419-022408

896 46. Falkowska E, Le KM, Ramos A, et al. Broadly neutralizing HIV antibodies define a glycan-
897 dependent epitope on the prefusion conformation of gp41 on cleaved envelope trimers.
898 *Immunity*. 2014;40(5):657-668. doi:10.1016/j.immuni.2014.04.009

899 47. Crispin M, Doores KJ. Targeting host-derived glycans on enveloped viruses for antibody-
900 based vaccine design. *Curr Opin Virol*. 2015;11:63-69. doi:10.1016/j.coviro.2015.02.002

901 48. Berndsen ZT, Chakraborty S, Wang X, et al. Visualization of the HIV-1 Env glycan shield
902 across scales. *Proc Natl Acad Sci U S A*. 2020;117(45):28014-28025.
903 doi:10.1073/pnas.2000260117

904 49. Antanasijevic A, Bowman CA, Kirchdoerfer RN, et al. From structure to sequence:
905 Antibody discovery using cryoEM. *Sci Adv*. 2022;8(3):eabk2039. doi:10.1126/sciadv.abk2039

906 50. Andrews SF, Huang Y, Kaur K, et al. Immune history profoundly affects broadly
907 protective B cell responses to influenza. *Sci Transl Med*. 2015;7(316):316ra192.
908 doi:10.1126/scitranslmed.aad0522

909 51. Inoue T, Kurosaki T. Memory B cells. *Nat Rev Immunol*. 2024;24(1):5-17.
910 doi:10.1038/s41577-023-00897-3

911 52. Torrents de la Peña A, de Taeye SW, Sliepen K, et al. Immunogenicity in Rabbits of HIV-1
912 SOSIP Trimers from Clades A, B, and C, Given Individually, Sequentially, or in Combination. *J*
913 *Virol*. 2018;92(8):e01957-17. doi:10.1128/JVI.01957-17

914 53. Zhao F, Joyce C, Burns A, et al. Mapping Neutralizing Antibody Epitope Specificities to an
915 HIV Env Trimer in Immunized and in Infected Rhesus Macaques. *Cell Reports*. 2020;32(10).
916 doi:10.1016/j.celrep.2020.108122

917 54. Dal Porto JM, Haberman AM, Kelsoe G, Shlomchik MJ. Very Low Affinity B Cells Form
918 Germinal Centers, Become Memory B Cells, and Participate in Secondary Immune Responses
919 When Higher Affinity Competition Is Reduced. *J Exp Med*. 2002;195(9):1215-1221.
920 doi:10.1084/jem.20011550

921 55. Taylor JJ, Pape KA, Steach HR, Jenkins MK. Humoral immunity. Apoptosis and antigen
922 affinity limit effector cell differentiation of a single naïve B cell. *Science*. 2015;347(6223):784-
923 787. doi:10.1126/science.aaa1342

924 56. Schiepers A, van ’t Wout MFL, Hobbs A, Mesin L, Victora GD. Opposing effects of pre-
925 existing antibody and memory T cell help on the dynamics of recall germinal centers. *bioRxiv*.
926 Published online December 15, 2023:2023.12.15.571936. doi:10.1101/2023.12.15.571936

927 57. Tas JMJ, Koo JH, Lin YC, et al. Antibodies from primary humoral responses modulate the
928 recruitment of naive B cells during secondary responses. *Immunity*. Published online August
929 2022:S1074761322003557. doi:10.1016/j.immuni.2022.07.020

930 58. McNamara HA, Idris AH, Sutton HJ, et al. Antibody Feedback Limits the Expansion of B
931 Cell Responses to Malaria Vaccination but Drives Diversification of the Humoral Response.
932 *Cell Host Microbe*. 2020;28(4):572-585.e7. doi:10.1016/j.chom.2020.07.001

933 59. Schaefer-Babajew D, Wang Z, Muecksch F, et al. Antibody feedback regulates immune
934 memory after SARS-CoV-2 mRNA vaccination. *Nature*. 2023;613(7945):735-742.
935 doi:10.1038/s41586-022-05609-w

936 60. Tas JMJ, Mesin L, Pasqual G, et al. Visualizing antibody affinity maturation in germinal
937 centers. *Science*. 2016;351(6277):1048-1054. doi:10.1126/science.aad3439

938 61. Viant C, Weymar GHJ, Escolano A, et al. Antibody Affinity Shapes the Choice between
939 Memory and Germinal Center B Cell Fates. *Cell*. 2020;183(5):1298-1311.e11.
940 doi:10.1016/j.cell.2020.09.063

941 62. Purtha WE, Tedder TF, Johnson S, Bhattacharya D, Diamond MS. Memory B cells, but
942 not long-lived plasma cells, possess antigen specificities for viral escape mutants. *J Exp Med*.
943 2011;208(13):2599-2606. doi:10.1084/jem.20110740

944 63. Ferguson JA, Raghavan SSR, Peña Alzua G, et al. Functional and epitope specific
945 monoclonal antibody discovery directly from immune sera using cryoEM. Published online
946 December 9, 2024. doi:10.1101/2024.12.06.627063

947 64. Schulte D, Šiborová M, Käll L, Snijder J. Simultaneous polyclonal antibody sequencing
948 and epitope mapping by cryo electron microscopy and mass spectrometry. *Elife*.
949 2025;14:RP101322. doi:10.7554/eLife.101322

950 65. Baba TW, Liska V, Hofmann-Lehmann R, et al. Human neutralizing monoclonal
951 antibodies of the IgG1 subtype protect against mucosal simian-human immunodeficiency
952 virus infection. *Nat Med*. 2000;6(2):200-206. doi:10.1038/72309

953 66. Guenaga J, de Val N, Tran K, et al. Well-ordered trimeric HIV-1 subtype B and C soluble
954 spike mimetics generated by negative selection display native-like properties. *PLoS Pathog*.
955 2015;11(1):e1004570. doi:10.1371/journal.ppat.1004570

956 67. Moore JP, Trkola A, Korber B, et al. A human monoclonal antibody to a complex epitope
957 in the V3 region of gp120 of human immunodeficiency virus type 1 has broad reactivity
958 within and outside clade B. *J Virol*. 1995;69(1):122-130. doi:10.1128/JVI.69.1.122-130.1995

959 68. Montefiori DC. Measuring HIV Neutralization in a Luciferase Reporter Gene Assay. In:
960 Prasad VR, Kalpana GV, eds. *HIV Protocols*. Vol 485. Methods in Molecular Biology. Humana
961 Press; 2009:395-405. doi:10.1007/978-1-59745-170-3_26

962 69. Li M, Gao F, Mascola JR, et al. Human immunodeficiency virus type 1 env clones from
963 acute and early subtype B infections for standardized assessments of vaccine-elicited
964 neutralizing antibodies. *J Virol*. 2005;79(16):10108-10125. doi:10.1128/JVI.79.16.10108-
965 10125.2005

966 70. Turner HL, Jackson AM, Richey ST, et al. Protocol for analyzing antibody responses to
967 glycoprotein antigens using electron-microscopy-based polyclonal epitope mapping. *STAR*
968 *Protoc*. 2023;4(3):102476. doi:10.1016/j.xpro.2023.102476

969 71. Pettersen EF, Goddard TD, Huang CC, et al. UCSF Chimera--a visualization system for
970 exploratory research and analysis. *J Comput Chem*. 2004;25(13):1605-1612.
971 doi:10.1002/jcc.20084

972 72. Pintilie GD, Zhang J, Goddard TD, Chiu W, Gossard DC. Quantitative analysis of cryo-EM
973 density map segmentation by watershed and scale-space filtering, and fitting of structures by
974 alignment to regions. *J Struct Biol*. 2010;170(3):427-438. doi:10.1016/j.jsb.2010.03.007

975 73. Zheng SQ, Palovcak E, Armache JP, Verba KA, Cheng Y, Agard DA. MotionCor2:
976 anisotropic correction of beam-induced motion for improved cryo-electron microscopy. *Nat*
977 *Methods*. 2017;14(4):331-332. doi:10.1038/nmeth.4193

978 74. Punjani A, Rubinstein JL, Fleet DJ, Brubaker MA. cryoSPARC: algorithms for rapid
979 unsupervised cryo-EM structure determination. *Nat Methods*. 2017;14(3):290-296.
980 doi:10.1038/nmeth.4169

981 75. Zhang K. Gctf: Real-time CTF determination and correction. *J Struct Biol*. 2016;193(1):1-
982 12. doi:10.1016/j.jsb.2015.11.003

983 76. Yang Z, Lasker K, Schneidman-Duhovny D, et al. UCSF Chimera, MODELLER, and IMP: an
984 integrated modeling system. *J Struct Biol*. 2012;179(3):269-278.
985 doi:10.1016/j.jsb.2011.09.006

986 77. Emsley P, Crispin M. Structural analysis of glycoproteins: building N-linked glycans with
987 Coot. *Acta Crystallogr D Struct Biol*. 2018;74(Pt 4):256-263.
988 doi:10.1107/S2059798318005119

989 78. Emsley P, Lohkamp B, Scott WG, Cowtan K. Features and development of Coot. *Acta*
990 *Crystallogr D Biol Crystallogr*. 2010;66(Pt 4):486-501. doi:10.1107/S0907444910007493

991 79. Wang RYR, Song Y, Barad BA, Cheng Y, Fraser JS, DiMaio F. Automated structure
992 refinement of macromolecular assemblies from cryo-EM maps using Rosetta. *Elife*.
993 2016;5:e17219. doi:10.7554/eLife.17219

994 80. Adams PD, Afonine PV, Bunkóczi G, et al. PHENIX: a comprehensive Python-based
995 system for macromolecular structure solution. *Acta Crystallogr D Biol Crystallogr*. 2010;66(Pt
996 2):213-221. doi:10.1107/S0907444909052925

997 81. Afonine PV, Poon BK, Read RJ, et al. Real-space refinement in PHENIX for cryo-EM and
998 crystallography. *Acta Crystallogr D Struct Biol*. 2018;74(Pt 6):531-544.
999 doi:10.1107/S2059798318006551

1000 82. Williams CJ, Headd JJ, Moriarty NW, et al. MolProbity: More and better reference data
1001 for improved all-atom structure validation. *Protein Sci*. 2018;27(1):293-315.
1002 doi:10.1002/pro.3330

1003 83. Barad BA, Echols N, Wang RYR, et al. EMRinger: side chain-directed model and map
1004 validation for 3D cryo-electron microscopy. *Nat Methods*. 2015;12(10):943-946.
1005 doi:10.1038/nmeth.3541

1006
1007
1008
1009
1010
1011